Diffusion of dissolved gases in chemically perturbed clay

Chloé Roonacker

Academic year 2021 - 2022

Promotor: ***Prof. Christophe Bruggeman, ULg***

Thesis submitted in partial fulfilment of the requirements for the degree of Master of Science in Nuclear Engineering

Belgian Nuclear Higher Education Network, c/o SCK•CEN, Boeretang 200, BE-2400 Mol, Belgium

Master of Science

in Nuclear Engineering

Thesis Summary Page

Name of the student:

Chloé Roonacker

Title:

Diffusion of dissolved gases in chemically perturbed clay

Abstract:

The thesis research is in the framework of safe geological disposal of high and intermediate-level radioactive waste, for which the Boom Clay is studied at the moment as the reference host formation in Belgium. Boom Clay would be a suitable host rock thanks to many beneficial properties, including its transport properties which are mainly dominated by diffusion as Boom Clay has a sufficiently low hydraulic conductivity. In previous work, the diffusion coefficient of gases in Boom Clay was studied because gas generation in a geological repository is unavoidable (corrosion of metals, radiolysis of water,...). Within this research, our focus lies on the geochemical perturbation of Boom Clay as a consequence of NaNO3 leaching from Eurobitumen bituminised waste. More concretely, we analyse the diffusion of 4 gases (He, CH4, Xe, and C2H6) and we evaluate how much their diffusion coefficients are changed after perturbation. It appears that the smallest diffusing molecule He, was very sensitive to the chemical perturbation. After the diffusion experiments, we characterized the samples to study the petrographical and petrophysical changes. With N2-adsorption measurements, we noticed that the specific surface area of the clay minerals had decreased to half of the expected value in the disturbed samples. Therefore we assume that the interlayer of the clay platelets are blocked due to NaNO3 perturbation and that this reduces the access of the interlayers. Our hypothesis is that He uses the interlayer as a pathway through the clay and when this interlayer is blocked due to NaNO3, the pathway of He is barred, which lowers the diffusion coefficient.

Promotor: Prof. Christophe Bruggeman

Mentor: Elke Jacops

Assessors: Prof. Manuel Sintubin
Prof. Nicolas Pauly

Approval for submission by promotor:

Christophe Bruggeman (Signature)

Digitally signed by Christophe Bruggeman (Signature)
Date: 2022.06.08 21:20:15 +02'00'

Academic Year 2021-2022

Belgian Nuclear higher Education Network, c/o SCK CEN, Boeretang 200, BE-2400 Mol, Belgium

Contents

Preface

In this master thesis, the diffusion of dissolved gases in chemically perturbed Boom Clay, as a result of $NaNO_3$, is studied. This is investigated to assess how much $NaNO_3$ has an impact on the diffusive transport properties. I already have a degree of Master in the Geology, and this thesis is submitted for a second degree of Master of Science in Nuclear Engineering, so I want to thank my promotor prof. Bruggeman, for giving me the opportunity to work on this interesting topic that combines both domains. Besides that, I could count on him for giving useful advice and feedback. Secondly, I want to thank my mentor Elke Jacops for her incredible guidance during this process and for her comments and feedback on my text. Thanks to her approachable attitude, I could always ask her help for minor and major problems I encountered. Before this project started, I had no experience with diffusion experiments, therefore I am thankful for Anneleen Vanleeuw, laboratory technician at SCK-CEN, who assisted me in this process with so much patience and learned me everything about the practical side of gas experiments.

I am very grateful for the help of so many people on the R&D Disposal group of SCK-CEN; Dorien Verhaegen and Tom Maes for helping me with the practical characterisation of the samples, Miroslav Honty and Nele Bleyen for their feedback during meetings, Lander Frederickx for his feedback but especially for his help with interpreting XRD and ICP data and at last, Norbert Maes for his advice, revising my text, feedback, and overall interesting suggestions. I want to thank Hannes Claes, who helped me with the NMR measurements at KU Leuven.

Next, I want to express my love and gratitude to my best friend and roommate Kaat for all her homemade dinners and all our laughs together, and to my partner Josha for the unconditional support and tolerating my mood swings once in a while. At last, I want to let my parents know that I could have never done this without them. They gave me the opportunity to study for an extra two years and their belief in me is immeasurable, I could not be more thankful.

Abstract

The thesis research is in the framework of safe geological disposal of high and intermediate-level radioactive waste, for which the Boom Clay is studied at the moment as the reference host formation in Belgium. Boom Clay would be a suitable host rock thanks to many beneficial properties, including its transport properties which are mainly dominated by diffusion as Boom Clay has a sufficiently low hydraulic conductivity. In previous work, the diffusion coefficient of gases in Boom Clay was studied because gas generation in a geological repository is unavoidable (corrosion of metals, radiolysis of water,...). Within this research, our focus lies on the geochemical perturbation of Boom Clay as a consequence of $NaNO_3$ leaching from Eurobitumen bituminised waste. More concretely, we analyse the diffusion of 4 gases (He, CH_4, Xe, and C_2H_6) and we evaluate how much their diffusion coefficients are changed after perturbation. It appears that the smallest diffusing molecule He, was very sensitive to the chemical perturbation. After the diffusion experiments, we characterized the samples to study the petrographical and petrophysical changes. With N_2-adsorption measurements, we noticed that the specific surface area of the clay minerals had decreased to half of the expected value in the disturbed samples. Therefore we assume that the interlayer of the clay platelets are blocked due to $NaNO_3$ perturbation and that this reduces the access of the interlayers. Our hypothesis is that He uses the interlayer as a pathway through the clay and when this interlayer is blocked due to $NaNO_3$, the pathway of He is barred, which lowers the diffusion coefficient.

Samenvatting

Deze master thesis sluit aan bij het RD&D-programma met trekking tot geologische berging van hoogradioactief en /of langlevend afval in een diepe kleiformatie in België. Diepe berging in de ondergrond wordt op dit ogenblik als de meest veilige en duurzame oplossing beschouwd, aangezien het radioactieve afval in een stabiele omgeving wordt geplaatst. Het afval wordt hierdoor afgescheiden van mens en milieu door een hele reeks barrières en de leefwereld wordt beschermd tegen de schadelijke effecten van het radioactieve afval. Het systeem is gebaseerd op het 'defense in depth' principe met 2 soorten barrières, waarbij de ene het overneemt wanneer de andere faalt; enerzijds is er de natuurlijk barrière, de stabiele geologische formatie waarin het afval zal geplaatst worden en anderzijds is er de kunstmatige barriere, bestaande uit de verschillende lagen rond het afval en de opvulmaterialen. Door de combinatie van de twee, zijn we goed beschermd doordat het afval wordt ingesloten door de kunstmatige barrière en nadat deze, na een lange tijd, wordt aangetast en de radioactieve stoffen zouden vrijkomen, zorgt de natuurlijk barrière voor een zeer trage verspreiding en afzondering.

De stabiele geologische formatie bestudeerd in België is de Boomse Klei, door verschillende gunstige eigenschappen is deze kleilaag geschikt voor geologische berging. Zo is de Boomse Klei weinig waterdoorlatend en verspreiden radioactieve stoffen zich zeer traag door de klei. Boomse Klei is ook plastisch, wat een goede eigenschap is wanneer er een scheur zou ontstaan in de kleilaag, omdat die zich dan vanzelf sluit. Daarbij is de Boomse Klei afgezet 30 miljoen jaar geleden en daardoor wordt deze beschouwd als stabiel over een geologische tijdschaal.

Wanneer het afval zou gestockeerd worden in de ondergrondse galerijen, is het onvermijdbaar dat er gas wordt geproduceerd. Dit is een resultaat van verschillende processen zoals radiolyse van water en andere organische verbindingen, anaërobe corrosie van metaal, radioactief verval en microbiele degradatie van organisch afval. Wanneer deze gasopwekking traag genoeg verloopt, kan het gas oplossen in het poriewater en diffundeert het weg. Echter, wanneer de gasopwekking de capaciteit van de diffuus transport overschrijdt, over-satureert het poriewater met gas en ontstaat er een vrije gasfase. Deze opbouw van vrij gas kan leiden tot een druk opbouw in de ondergrondse galerijen, die schadelijke gevolgen kan hebben en nefast zijn voor de veiligheid functies. Daarom is het dus zeer belangrijk dat er onderzoek wordt gedaan naar gasopwekking en gasafvoer in Boomse Klei. Doordat Boomse Klei weinig waterdoorlatend is, is gasafvoer voornamelijk gedomineerd door diffusie en de diffusie coëficiënt bepaalt de snelheid van dit transport in de kleilaag. De diffusie coëficiënt van verschillende gassen in onverstoorde Boomse Klei is dus in het

verleden al bestudeerd.

Het probleem aangekaart in deze master thesis is het verstoren van de Boomse Klei door gebituminiseerd radioactief afval. Eurobitumen gebituminiseerd afval is een medium level radioactief afval, geproduceerd in België en zou dus potentieel gestockeerd worden in de diep geologische berging. Het risico verbonden aan dit type afval is opgedeeld in twee categoriën: geochemisch en geomechanische verstoringen. De geochemische verstoringen zijn een gevolg van $NaNO_3$, dat lekt uit het afval. In dit onderzoek hebben we het effect van $NaNO_3$ op diffusie gedomineerd transport in de Boomse Klei bestudeerd. De diffusie coëficiënt van 4 gassen (He, CH_4, Xe en C_2H_6) in verstoorde Boomse Klei is verkregen en de doelstelling is om te evalueren of de transport eigenschappen van Boomse Klei worden beïnvloed door $NaNO_3$.

Na de diffusie experimenten op verstoorde klei stalen, hebben we de stalen op verschillende manieren gekarakteriseerd om te analyseren of er petrografische of petrofysiche veranderingen te zien zijn en om deze eventuele veranderingen te linken aan het diffusie transport.

List of Figures

List of Tables

List of abbreviations

µ-CT	µ-Chromatography
BET	Brunauer, Emmet and Teller
CEC	Cation exchange capacity
EBS	Engineered barrier system
EDL	Electrical double layer
HTO	Triated water
ICP	Inductively coupled plasma
NA	Not Available
NM	Not Measured
NMR	Nuclear magnetic resonance
RD&D	Research development and demonstration
SSA	Specific surface area
XRD	X-ray diffraction

List of symbols

A	Cross-sectional area (m^2)
c	Concentration in porous medium (mol/m^3)
D_0	Diffusion coefficient in water (m^2/s)
D_{app}	Apparent diffusion coefficient (m^2/s)
D_{eff}	Effective diffusion coefficient (m^2/s)
D_p	Pore diffusion coefficient (m^2/s)
dV/dt	Inflow rate (m^3/s)
F	Flux (mol/m^2s)
G	Geometric factor (-)
K	Hydraulic conductivity (m/s)
$l/\Delta P$	Length of plug over pressure gradient
m	Massa (g)
R	Retardation factor (-)
R_{pore}	Pore width (m)
SSA	Specific surface area (m^2/g)
t	Time (s)
x	Length (m)
X_i	Number of absorbed gas molecules
wt%	weight percentage (%)
δ	Constrictivity (-)
η	Porosity (-)
θ	Angle (°)
λ	Wavelength (nm)
ρ	Density (g/l)
σ	Kinetic diameter (m)
τ	Tortuosity (-)

1 Introduction

Deep geological disposal is seen as a proper solution for the long-term management of high- and intermediate level radioactive waste in many countries. There has been no formal decision taken for the final disposal in Belgium, however, this option is considered for waste of category B and C. Cat B&C are long-lived and/or high-level radioactive and present risks on a timescale of tens to hundreds of millennia as a result of the high quantity of long-lived radionuclides. The management of radioactive waste in Belgium is under the competence of ONDRAF/NIRAS.

Since the risks are present for such a long timescale, there is a need for a long-term disposal facility, in a deep, stable environment. By emplacing the waste in a geological repository, in an engineered barrier system, the people and the environment are protected from the harmful effects, see Figure 1.A (ONDRAF/NIRAS Research, 2012). The system is thus based on an engineered barrier system (EBS), which has as function to contain the radioactive waste physically and prevent the dispersion of contaminants. The current engineered EBS for intermediate level waste is the monolith B, including the different drums surrounded by a concrete container. In Figure 1.B the monolith B is pictured in detail, and is made of mortar and cement. The disposal galleries are made of concrete lining for mechanical stability. The monoliths are gathered in the tunnels and the retrieved gap is filled with cement backfill, improving the integrity of the waste package against steel corrosion thanks to its high pH buffering capacity over a long period (Bel et al., 2006; ONDRAF/NIRAS Research, 2012).

The disposal system makes further use of a natural barrier, namely the stable geological formation, retarding the migration of the radionuclides when the EBS fails or degrades. The natural barrier has a second function, it isolates the waste from inadvertent human intrusion. In Belgium, the Boom Clay Formation qualifies as a proper host rock for the repository. This formation is deposited 30 million years ago and is assumed to be stable over a geologically long timescale. In Mol-Dessel, the reference site for RD&D in Boom Clay where the HADES underground research facility is located, Boom Clay is present at a depth of 190-290 meters, attaining a 100 meter thickness. For long term geological disposal, Boom Clay has certain beneficial properties, such as a high sorption capacity for many radionuclides retarding the migration, a low hydraulic conductivity, and self-sealing properties (Yu et al., 2013; Wemaere et al., 2008; Altmann et al., 2012; OECD, 2003; Van Geet et al., 2008).

After closure of the repository, it is inevitable that gas generates around the waste as

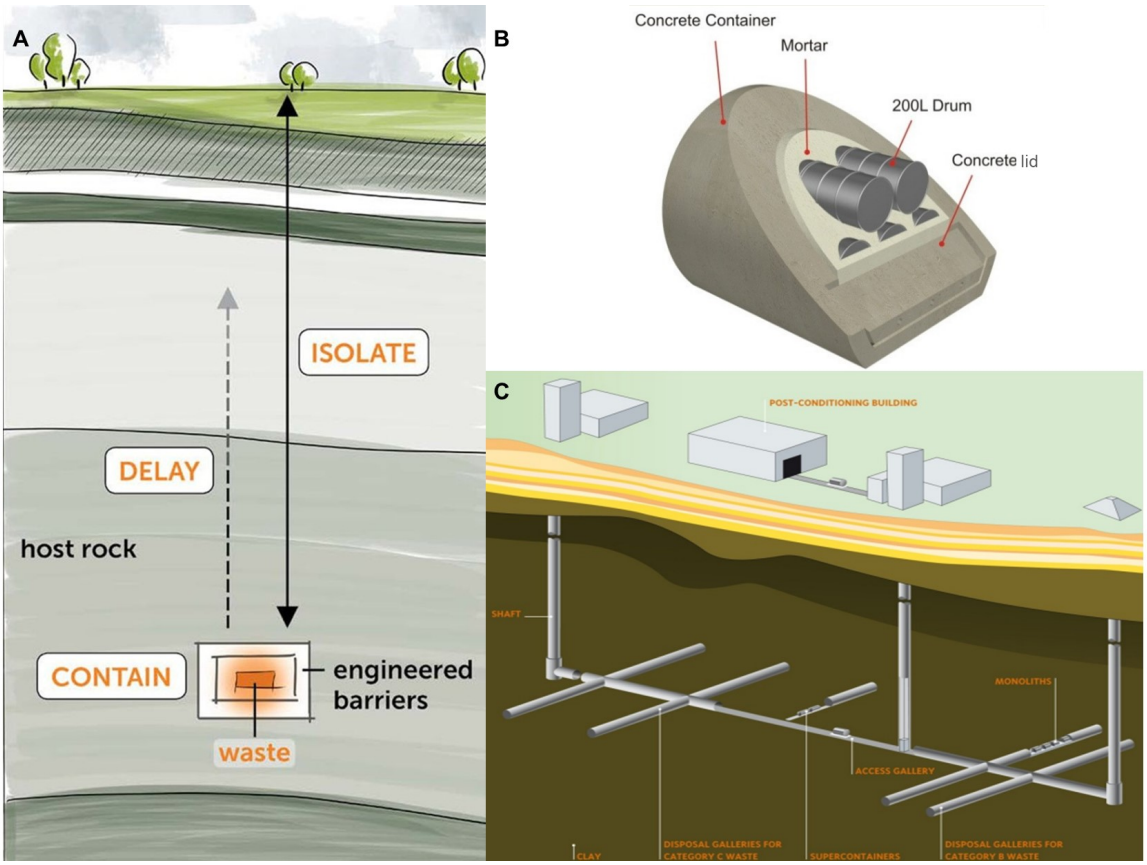

Figure 1: A) The engineered barrier systems around the radioactive waste physically contains the waste and the stable geological formation working as a natural barrier to delay the substances that could be released if the EBS fails and isolate it from human intrusion(Norris, 2017). B) Monolith B for intermediate level waste C) Picture of the potential geological repository and the surface facility (ONDRAF/NIRAS Research, 2012).

a consequence of multiple processes such as radiolysis of water and organic compounds, anaerobic corrosion of metals, radioactive decay, and microbial degradation of organic waste (Shaw, 2015; Perko & Weetjens, 2011; Rodwell et al., 1999). If gas generation is sufficiently slow, the gas dissolves in the pore water and diffuses away. However, if the gas production rate exceeds the capacity of diffusive transport, pore water becomes oversaturated and a free gas phase occurs. The build-up of free gas could subsequently lead to a pressure buildup in the repository, resulting in detrimental effects that have an influence on the safety functions. More specific it might cause local damage to the barriers, which could result in a potential, preferential water pathway and contaminated water could be expelled from the repository into the host rock formation (Perko & Weetjens, 2011). The balance between gas production and gas diffusion is an important measure to whether or not the disposal system would be subjected to these detrimental effects.

In the research that focuses on Boom Clay as host rock formation, it is therefore important to study the processes of gas generation and gas dissipation. As mentioned above, Boom

Clay has a low permeability and low hydraulic gradient, therefore transport of gases is predominantly diffusion-driven and the diffusion coefficient of the dissolved gases defines the rate of transport in the natural barrier. In previous studies, the diffusion coefficients of different gases in undisturbed Boom Clay are obtained with a double through-diffusion experiment, which was developed by Jacops et al. (2015).

A problem arises for a certain type of radioactive waste, namely for bituminised waste, that could possibly disturb the Boom Clay layers. Eurobitumen bituminised is an intermediate level radioactive waste, produced in Belgium, and will potentially be disposed in the waste facility. The possible risks associated with this type of waste are divided into two categories, i.e. geochemical and geomechanical disturbances. The geochemical disturbance is a result of $NaNO_3$ leaching from the Eurobitumen bituminised radioactive waste. These geochemical perturbations in Boom Clay are studied in the Long Term Experiment of Bleyen et al. (2018), under supervision of SCK-CEN.

Within this research, the effect of $NaNO_3$ on the diffusion-dominated transport of gases in Boom Clay is studied. The diffusion coefficient of 4 gases He, CH_4, C_2H_6, and Xe in perturbed Boom Clay is obtained by applying the developed double-through diffusion experiment. The objective is to evaluate whether the transport properties of Boom Clay are affected by $NaNO_3$ perturbation. For this double-through diffusion experiment, the perturbed Boom Clay sample studied in the Long Term Experiment is analysed.

In addition, the diffusion coefficients of the 4 gases in disturbed Eigenbilzen Sand are compared to the diffusion coefficients in undisturbed Eigenbilzen Sand, to better understand the process of $NaNO_3$ perturbation on transport properties. Eigenbilzen Sand is a more silt-enriched formation, overlying the Boom Clay (Vandenberghe et al., 2001).

After acquiring the diffusion coefficient of the 4 gases in chemically disturbed Boom Clay and Eigenbilzen Sand and undisturbed Eigenbilzen Sand, all samples are characterized with various techniques. The porosity is recalculated by drying the samples. The mineralogical composition is obtained by X-ray diffraction (XRD). With N_2-adsorption, the specific surface area of the samples and the available pore volume is evaluated. The porosity, pore size distribution, and water saturation are estimated with Nuclear Magnetic Resonance (NMR). Finally, to verify the Na-occupancy of the chemically perturbed samples, the CEC is calculated by the Cu-trien method. All the methods are further described in Chapter 5.3.

To conclude, the main purpose of the research is to assess if leaching of $NaNO_3$ from Eurobitumen bituminised radioactive waste has an influence on diffusion-driven transport of gases.

2 Boom Clay

2.1 Geological setting

The Rupelian Boom Clay formation is deposited in the Campine Basin, which is the southern part of the North Sea Basin (Vandenberghe et al., 2014). During the Rupelian, the Lower Oligocene, this was a shallow marine environment with depths between 50 and 100 m. Boom Clay has an alternating banded structure of clayey silt and silty clay layers, see Figure 3, a result of the periodical change of the depositional characteristics (Mertens et al., 2003). The Rupel Group strata occur at the subsurface in Northern Belgium, along the Scheldt and Rupel rivers towards the Meuse river in the east (Vandenberghe et al., 2001). It forms a wide belt of 5 to 15 km, interrupted in the middle in the Hageland (Honty et al., 2022). In figure 2, the outcrop area of Boom Clay is indicated on the map of the Northern part of Belgium.

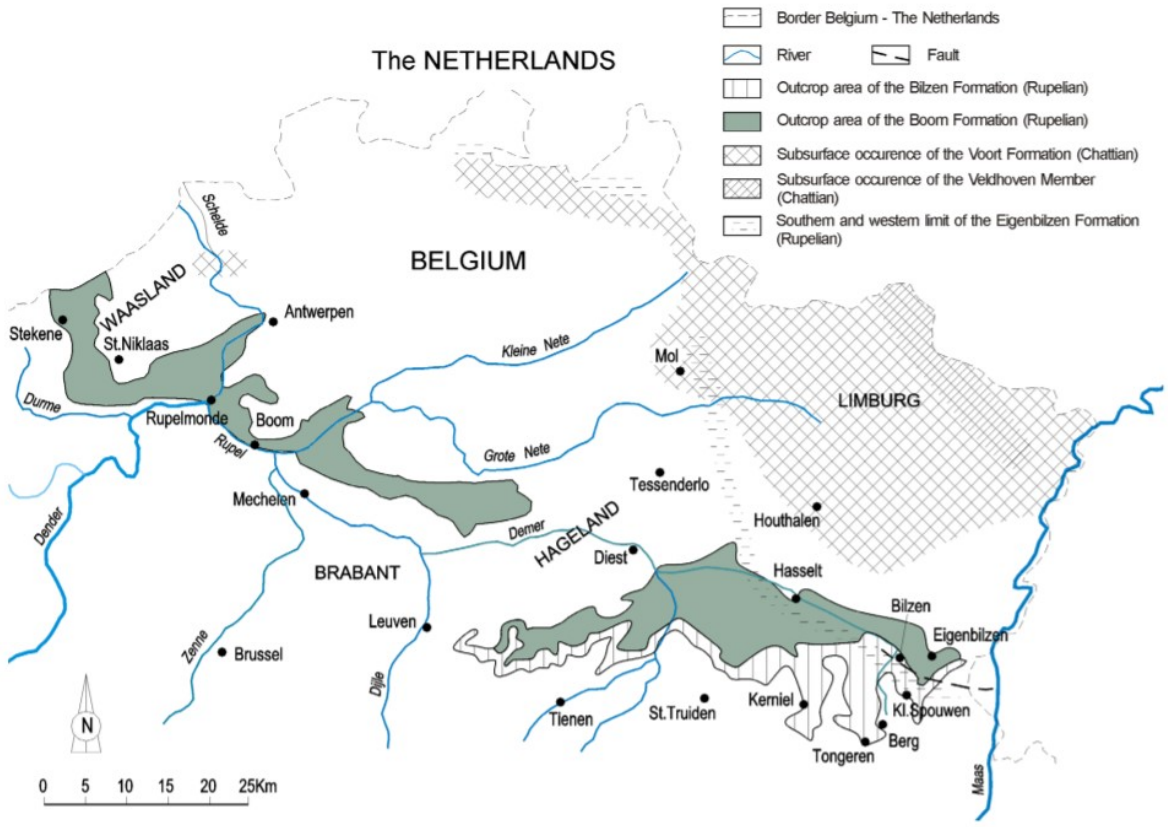

Figure 2: Boom Clay formation at the subsurface in the Northern part of Belgium (Vandenberghe et al., 2001)

Figure 3: Alternating layers of clay and silt in the Boom Clay outcrop in Terhagen-Rumst (Vandenberghe et al., 2014).

2.2 Mineralogy

Boom clay is characterized by a mineralogical composition of 23 to 59 wt% clay minerals (illite, smectite, interstratified illite-smectite mixture, and kaolinite), 23 to 55 wt% quartz, 10 to 13 wt% feldspars, 1 to 3 wt% carbonates, 1 to 2 wt% pyrite, and 1 to 5 wt% organic carbon (Frederickx et al., 2018). The main clay-mineral fraction consists of 2:1 clay minerals illite and smectite. These phyllo-silicates are composed of TOT layers; two silica tetrahedral sheets with an alumina octahedral sheet in between, as seen in Figure 4. TOT clay minerals typically have a negative charge due to isomorphic substitutions of tetrahedral and octahedral metals. The most common isomorphic substitutions are the replacements of Si by Al in the tetrahedral sheets and the replacements of Al by Mg or Fe in the octahedral sheets. The location of these substitutions is not necessarily spatially ordered but can be randomly distributed, ordered, or clustered. The negative charge is counterbalanced by adsorption of cations, dissolved in the clay pore water, commonly alkali and alkaline earth metals such as Na^+, K^+, Ca^{2+} and Mg^{2+} (Tournassat et al., 2015). In addition, the negative charge is pushing anions further away from their surfaces into the clay pore water. The process results in a heterogeneous charge distribution in the pore water, surrounding the mineral surface, forming the Electrical Double Layer (EDL), the layer attracted to the negative surface by electrical charge, illustrated in Figure 5. There are two parameters controlling the thickness of the EDL; the nature of the ions

in the pore water and their concentration. EDL is thicker for monovalent ions than for divalent ions and decreases with higher ion concentration (high ionic strength) (Moors, 2005).

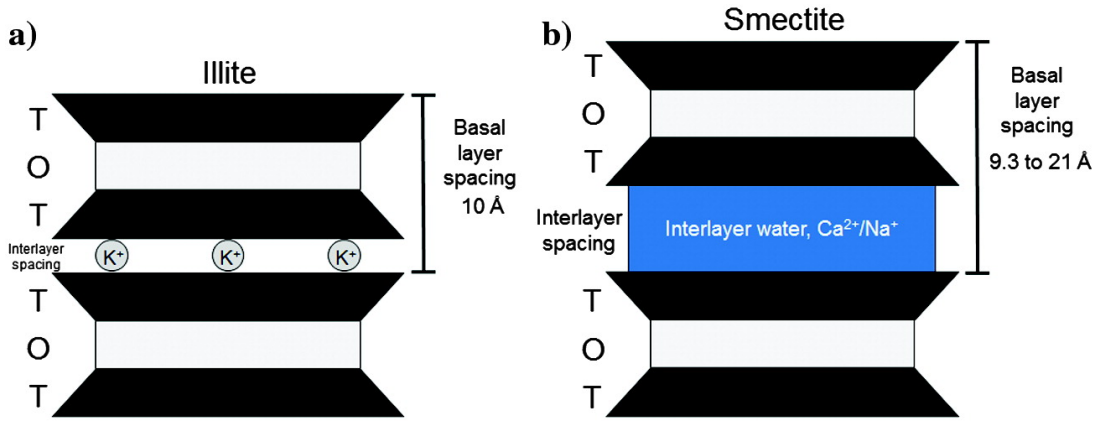

Figure 4: TOT-structure of a) illite with K^+ ions in the interlayer spacing and b) smectite with water, Ca^{2+}, and Na^+ in between the TOT layers (Xuan et al., 2019).

Illite and smectite have a similar unit structure, nevertheless, they differ significantly in their layer stacking and hydration properties. Illite is classified as a non-swelling clay mineral and is usually built up of 5 to 20 TOT-layers. For smectite, which is classified as swelling clay, the layers can become entirely delaminated. The interlayer space is occupied by cations, balancing the negative charge of the clay surface. In the non-swelling clay minerals, the cations present in the interlayer space are non-dissolved and predominantly poorly hydrated potassium cations. On the other hand, swelling clay minerals such as smectite, contains water in variable quantity in the interlayer space, as a consequence of multiple hydration spheres. The amount of water is a function of various parameters as temperature, ionic strength, relative humidity, or applied stress. The amount and identity of interlayer cations strongly influence the interlayer water molecules. Usually, the cations in the interlayer space in swelling clay minerals tend to be entirely dissolved. In Figure 6, a schematic representation of interlayer water, double layer water, and 'free water' in compacted bentonite from Bradbury & Baeyens (2002) is shown. The figure illustrates that pore space in compacted clay, as Boom Clay, is divided in interlayer space (between TOT-layers) and interparticle space (between clay stacks and/or between other mineral crystals present).

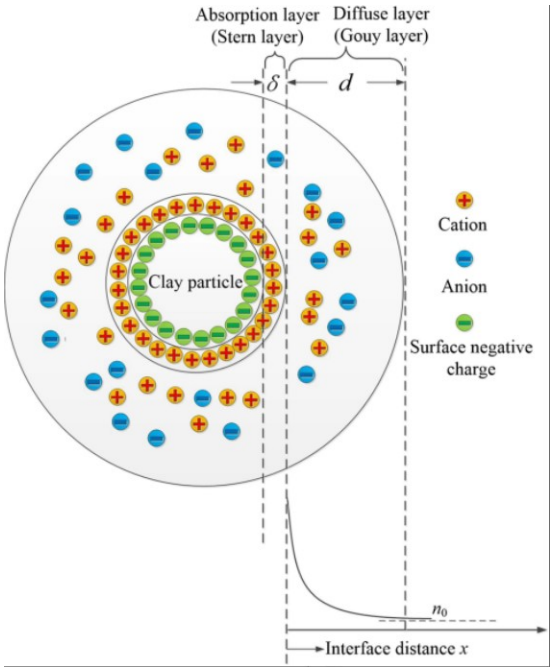

Figure 5: Schematic drawing of the electrical double layer around clay minerals (Jin et al., 2020).

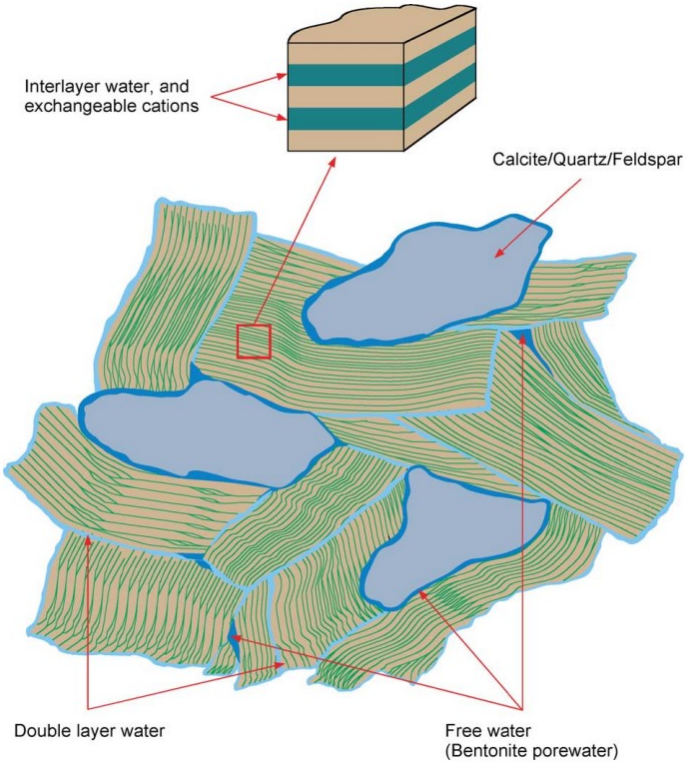

Figure 6: Schematic representation of interlayer water, double layer water, and "free water" in compacted bentonite from Bradbury & Baeyens (2002).

2.3 Geological disposal

Boom Clay is the reference host formation in Belgium for deep geological disposal of intermediate and high-level radioactive waste. This is due to several beneficial properties of Boom Clay. Firstly, Boom Clay has a low hydraulic gradient and low hydraulic conductivity which leads to slow water movement in the clay layers (Wemaere et al., 2008; Yu et al., 2013). Therefore, transport of dissolved species, gas, and radionuclides, happens predominantly via molecular diffusion (Altmann et al., 2012; OECD, 2003). As explained in the Chapter above, Boom Clay consisting mainly of illite and smectite has a high adsorption capacity as a consequence of isomorphic substitutions. This characteristic gives rise to retardation of positively charged radionuclide migration (Altmann et al., 2012; Maes et al., 2004). Due to the plasticity of the clay, the clay is self-sealing, which is favorable if a crack might occur in the surroundings of the waste disposal, through which water with radionuclides could be transported (Van Geet et al., 2008). Lastly, the environmental conditions prevailing in Boom Clay are rather beneficial for the storage of radioactive waste. The presence of pyrite results in a reducing environment. The reducing conditions and neutral to slightly alkaline pH imply a low solubility for radionuclides, which delays the migration of the radionuclides (Honty et al., 2022; Maes et al., 2004).

3 Eurobitumen bituminised radioactive waste

The EUROCHEMIC/Belgoprocess reprocessing facility produced circa 3000 m^3 bituminised radioactive waste, so-called Eurobitumen, during the seventies. This intermediate level radioactive waste incorporates the precipitation sludges, formed when chemically reprocessing spent nuclear fuel. It is a rather important radioactive waste form in Belgium, considering its high specific activity of 5.5 GBq beta/gamma and 0.25 GBq alpha per kg bituminised waste product and its large volume. The waste consists of a 60 wt% hard, blown bitumen matrix Mexphalt RB5/40 in which salt crystals, mainly $NaNO_3$ (20-30 wt%) and $CaSO_4$ (4-6 wt%), and residual water (0.5-1 wt%) are homogeneously dispersed. The waste contains small amounts of CaF_2, $Ca_3(PO_4)_2$, $Ni_2[(Fe, Mn)(CN)_6]$ and (hydr)oxides of Zr, Al, and Fe. The quantity of radionuclides is lower than 0.2 wt% and includes U and Pu isotopes, ^{241}Am, ^{244}Cm,^{60}Co, ^{90}Sr, and ^{137}Cs (Valcke et al., 2009).

The downside of this type of intermediate-level waste form is that it might affect the barrier function of the clay in two different ways

1. Geomechanical disturbance as a result of swelling of the waste leading to increased stress in the clay. Swelling is caused by osmosis-induced uptake of water or by gas generation during anaerobic corrosion of the steel waste drums, microbial activity and radiolysis (Bleyen et al., 2018).

2. Geochemical disturbance caused by the presence of dehydrated and hygroscopic salts which will lead to the dissolution of large amounts of soluble salts such as $NaNO_3$ and by the release of complexing and water-soluble organic compounds, which originate from chemical and radiolytic degradation of the bitumen (Mariën & Valcke, 2013).

For this research, the focus lies on the release of $NaNO_3$ in Boom Clay and its possible perturbing influence on the transport properties of gases.

4 Effect of $NaNO_3$ on Boom Clay

The favourable characteristics of Boom Clay as host rock for geological disposal are affected in different ways by leaching of $NaNO_3$. It could affect its performance by the increase of ionic strength, by inducing cation exchange between the clay cations and sodium, by oxidation of the redox-active Boom Clay components and by a change in microstructure. All perturbations are further elaborated in the next sections (Bleyen et al., 2018).

4.1 Increase ionic strength

The increase in ionic strength due to $NaNO_3$ has different consequences for Boom Clay. The surface charges are better shielded when the ionic strength is high, which results in a thinner electric double layer (EDL). The electrical potential profile $\Psi(x)$ is given by

$$\Psi = \Psi_0 e^{-kx} = \Psi_0 e^{-a\sqrt{I}x} \tag{1}$$

With Ψ_0 the electric potential at the surface, a is the proportionality constant, k is a physical constant, referred to as the Debye–Hückel parameter where $1/k$ corresponds to the thickness of the double layer, and I is the ionic strength (Qu & Li, 2000). The reduced thickness of the EDL causes a weaker repulsion of the anions and it could have an influence on the hydraulic conductivity, the filtration or retention capacity of larger mobile organic molecules, the compaction degree, and thus also on the migration of radionuclides.

A higher ionic strength signifies an increased concentration of electrolytes in the solution, which could have an effect on the solubility of the radionuclides. The equilibrium constant of the dissolution reaction indicates the change in solubility and can be acquired by the product of the activities of the ions in which the radioactive salt dissolves. This activity of an ion in a solution is given by

$$a_c = \gamma \frac{[C]}{[C^\theta]} \tag{2}$$

With γ defined as the activity coefficient, C is the molar concentration, and C^θ the concentration of the chosen standard state. The activity coefficient of the ions increases or decreases depending on the ionic strength of the solution. At low ionic strength, an increase will induce a decrease of the activity coefficient and results in an increased solubility. Whereas at high ionic strength, an increase will lead to an increase of the activity coefficient and thus a decrease in solubility. The point defining the low/high ionic strength and thus the turning point for the decrease/increase of the activity coefficient is dependent on the valency and the size of the ion (Liang et al., 2021). The degree

of solubility of radionuclides determines the migration of a radioactive waste disposal site.

At last, the increase of ionic strength could possibly cause a water flow towards the disposal galleries induced by a chemical gradient. The chemical-osmosis water flows with Boom Clay acting as a low-efficient semi-permeable membrane results in a local increase in pore water pressure and may create a risk if this high pore water pressure damages the waste disposal site. In-situ experiments in Boom Clay have been accomplished and the presently observed increased pressure due to chemical osmosis is too low to cause a considerable mechanical impact on the disposal gallery (Garavito et al., 2007; Valcke et al., 2010).

4.2 CEC of sodium and clay cations

Degradation of the waste leads to a release of sodium cations entering in the clay, which will exchange with cations on cation exchange sites. Ca^{2+}, Mg^{2+}, and K^{+} at the outer-layer surface are exchanged by Na^{+}, thickening the EDL. The hydrated radius of Na^{+} is 10% larger than the radius of K^{+} and two monovalent sodium cations are needed to exchange one divalent calcium or magnesium cation (Berkowitz et al., 2008). The expectation is that the CEC remains unchanged when disturbed by a high concentration of $NaNO_3$, although the EDL will change.

Cation exchange capacity of Na^{+} has another consequence for the barrier function of the clay. Due to the competition of sodium cations in the pore water, the sorption of radionuclides decreases and results in lower retardation. This affects solely the cationic radionuclides, which are primarily monovalent or divalent and unhydrolysed. Since the retardation for these types of radionuclides is dominated by cation exchange. In contrary, the retardation of multivalent and hydrolysed radionuclides is mainly controlled by surface complexation (Bleyen et al., 2018).

4.3 Oxidation of the redox-active Boom Clay

As explained in Chapter 2.3, the reducing capacity of Boom Clay is one of the beneficial characteristics for long term geological disposal of intermediate radioactive waste. Redox-sensitive radionuclides (as Se, Tc, and U) tend to be in their reduced form in the disposal environment. A more reduced state generally results in species that have a lower solubility, hence, a lower concentration in water and thus less available for transport (Bruggeman et al., 2010; De Cannière et al., 2010).

Leaching of $NaNO_3$ in the clay layers core results in oxidation of redox-active Boom Clay components due to abiotic and microbially NO_3^- reduction (Jørgensen et al., 2009; Bleyen et al., 2016). This redox reaction decreases the reducing capacity of Boom Clay, increasing the mobility of the radionuclides.

4.4 Change in microstructure

The sodium cations can be trapped between the clay particles and change the microstructure of the clay by swelling, dispersion, or slaking. slaking is the process of larger clay aggregates breaking into smaller microaggregates. If dispersion and slaking occur together, the interparticle space decreases and the EDLs will overlap. This overlapping might result in immobile pore water and therefore a lower hydraulic conductivity. These micro-structural changes could possibly affect the hydromechanical properties and therefore also the beneficial characteristics of the Boom Clay (Bleyen et al., 2018).

4.5 Conclusion

From the discussion above, clearly, $NaNO_3$ might have a negative effect on the barrier function of Boom Clay. This is because (1) EDL thickness is influenced and therefore also the hydraulic conductivity, anion exclusion, filtration capacity, and migration parameters of radionuclides might be affected; (2) sorption potential for positively charged radionuclides decreases; (3) the microstructure is affected by the sodium concentration, disturbing the hydromechanical properties of the clay.

The other processes are assumed to be of less importance, as the solubility of the radionuclides, or to have a beneficial influence, as the CEC results in a lower hydraulic conductivity (Bleyen et al., 2018).

5 Materials and methods

5.1 Samples

Boom Clay

The Boom Clay sample, 'NaNi H4', from the core sample with reference AG R4-5 Core 3.4 (9.31-9.54) was taken on 30/05/1996 and is parallel to the bedding. The borehole originates from the HADES underground research laboratory, which is situated in the Boom Clay layer at a depth of 225 meters, in Mol. More specific, the core is taken from the Andra Gallery, between ring 4 and 5, at a depth of 9.31 to 9.54 meter from the gallery. The HADES laboratory has an essential role in the research of safety and feasibility of geological disposal of radioactive waste. NaNi H4 is a sample analysed and studied in the Long Term Experiment in order to evaluate the geochemical perturbations of Boom Clay due to $NaNO_3$.

Eigenbilzen Sand

The second sample analysed is Eigenbilzen Sand, this is the sandy unit overlying the Boom Clay. The sand is deposited in the Early Oligocene and is characterized by a dark green, glauconite-rich, clayey sand with bioturbation. The formation consists of a clear alternating banded structure of coarser and finer grain sizes. Due to the overall coarser grain size, in comparison to Boom Clay, transport of dissolved gases and water is enhanced (Jacops et al., 2020). The sample, Mol-2A, is taken on 06/11/2014 from the core with reference ON-MOL2A-189 at a depth of 295.52 to 296.47 meter, perpendicular to the bedding. The borehole is executed from the surface in Mol. The Eigenbilzen Sand sample needs to be percolated with 1 M $NaNO_3$ to be chemically disturbed for 1 diffusion experiment, this is further explained in Chapter 5.2.1. A third diffusion experiment is done with a second sample of the ON-MOL2A-189, however, this sample is not percolated.

5.2 Diffusion experiment

To evaluate how the chemical perturbations have an effect on the transport properties of dissolved gases in Boom Clay, the double-through diffusion technique is applied (Jacops et al., 2013). The principle idea is to place the sample, a perturbed clay core, in a stainless steel cell in between two water vessels, which are pressurized with 2 mixtures of two different gases on each side. See figure 7 for the setup of the double-through diffusion experiment. During the diffusion test, the four dissolved gases will diffuse simultaneously from the high concentration compartment towards the low concentration compartment

of the diffusion cell. The two gas mixtures utilized in this experiment consist of He in combination with CH_4 and Xe mixed with C_2H_6.

5.2.1 Sample conditioning

The first step of the sample preparation is loading the sample in a stainless steel diffusion cell with a hydraulic press. This diffusion cell has a diameter of 38 mm and a height of 20 mm. The plasticity of the clayey samples ensures absolute sealing between sample and diffusion cell, which is crucial for a successful experiment. For a proper contact between clay and gas saturated water, a porous stainless steel filter plate with a diameter of 38 mm, a thickness of 2 mm, and a porosity of 40% is placed on both sides of the clay core. (Jacops et al., 2013).

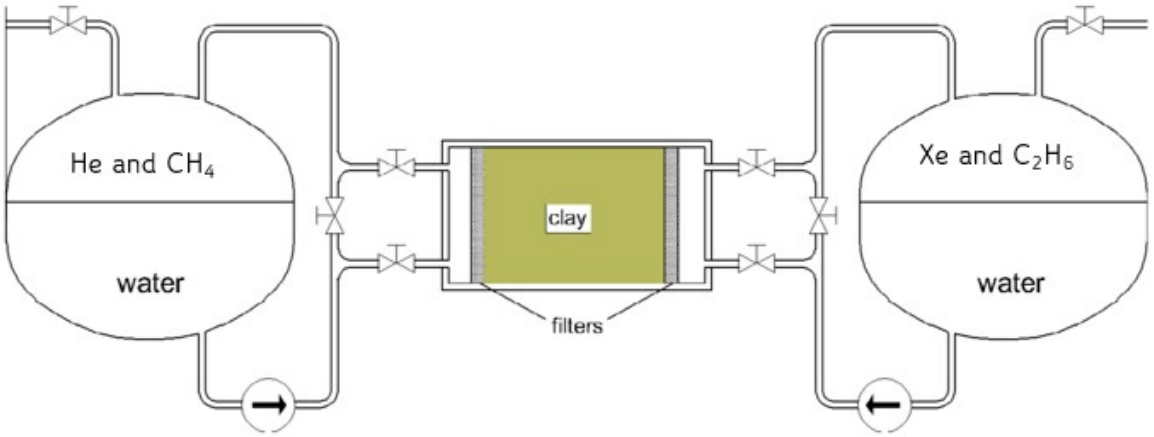

Figure 7: Double-through diffusion experiment with 4 dissolved gases (Jacops et al., 2015)

The research objective is to analyze the influence of the chemical perturbation on the barrier function of the clay, specifically, the transport of gases. So before setting up the experiment, the sample must be chemically disturbed, this is done with percolation of 1 M $NaNO_3$. The pore volume of the samples must be replaced a sufficient amount of times to reach a certain cation exchange occupancy. The NaNi H4 sample originates from the Long Term Experiment and the percolation has started on 14/03/2000 with 0.1 M $NaNO_3$, the concentration has been raised to 0.5 M on 21/08/2002 and to 1 M $NaNO_3$ on 20/07/2007. The Eigenbilzen Sand sample is a newly conditioned sample, percolation of Mol2A-189 started 04/02/2022. Mol2A-189 has a total volume of 23 ml and a porosity of 38%. To reach a Na^+-occupancy of 90%, the pore volume needs to be replaced 10 times, see figure 8. Therefore, 86 ml of 1 M $NaNO_3$ needs to pass through the core sample. The process is speeded up with the help of a syringe pump at a pressure of 1.5 bar.

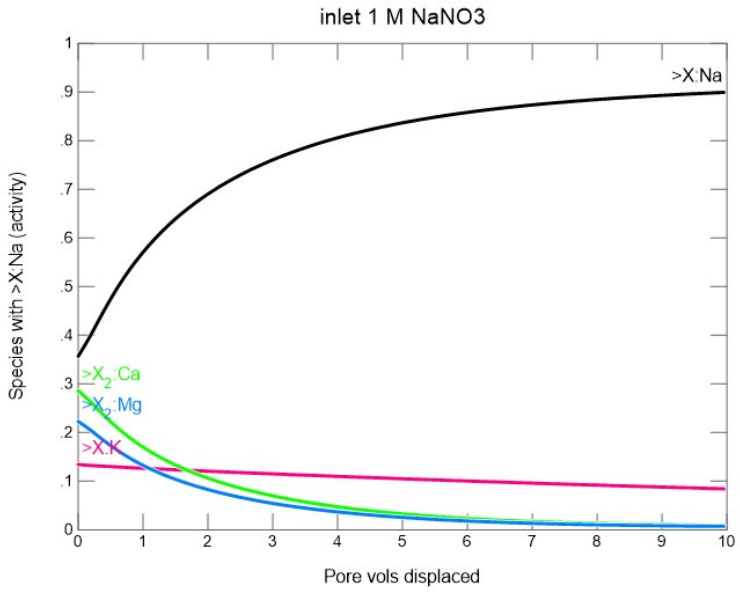

Figure 8: Cation exchange occupancies as function of displacement of pore volumes of inlet pore waters. Inlet concentrations of 1 M $NaNO_3$ (Wang, 2022).

The hydraulic conductivity of the samples is measured as a quality check prior to the start of the experiment. The test assures full saturation and verifies the sealing conditions of the sample in the cell. The hydraulic conductivity K is determined by injecting synthetic pore water with 1 M $NaNO_3$ during the percolation of the samples of NaNi H4 and Mol2A. For the hydraulic conductivity of the non-disturbed Mol2A sample, synthetic pore water with 0.014 M $NaHCO_3$ is used. The K-value is then determined by applying Darcy's Law (Wemaere et al., 2008).

$$K = \frac{1}{A}\frac{dV}{dt}\frac{l}{\Delta P} \tag{3}$$

With A the area of the cross-section of the clay core in m^2, dV/dt the inflow rate in m^3/s, and $l/\Delta P$ the length of the plug over the pressure gradient. The pressure is expressed in m water column and corresponds to approximately 8 bar for Boom Clay and 1 bar for Eigenbilzen Sand. Regular measurements are taken until the K-value is stable for 5 successive measurement intervals.

The water vessels are filled with 500 ml of synthetic pore water, which resembles the main constituents and the ionic strength of Boom Clay pore water and $NaNO_3$ is added to continuously disturb the samples. It is a solution of oxygen-free water with 0,014 mol/l $NaHCO_3$ and 1 mol/l $NaNO_3$.

The water vessels are pressurized at 6 to 10 bar with 500 ml gas mixtures of He and CH_4 in one water vessel, and Xe and C_2H_6 in the other water vessel. The gases dissolve in the synthetic pore water according to Henry's Law, resulting in an equilibrium between the free gas in the gas phase and the dissolved gas in the water. Therefore the diffusion of dissolved gases is measured.

The pumps over the clay core need to provide a constant low flow rate during the experiment, to provide a constant refreshment. Therefore, the pumps are calibrated for a flow rate of ± 10 ml/min.

It is important that the vessels are pressurized at the same pressure for multiple reasons; firstly, to prevent an advective flux, as only diffusion transport is of interest for the measurements. Besides, a pressure gradient could also cause a crack in the sample, damaging the sample and leading to a preferential pathway for the dissolved gas. Secondly, to guarantee the water saturation of the sample. The pressure should also remain constant since an advective, harmful flow could be the consequence of a leak in one of the vessels and in addition, a leak could influence the measurements. Therefore a leak test is performed before the start of the experiment, during this test the pressure is monitored for 48h, and the setup is considered leak tight if the pressure has not decreased. The valves between the water vessels and the clay core remain closed during the leak-test to avoid the ingress of dissolved gas before the start of the diffusion test (Jacops et al., 2013).

5.2.2 Diffusion measurement

A first sample is taken before opening the valves to determine the initial gas composition. Finally, the double-through diffusion experiment can start and the valves are opened. The water on both sides is circulated through the filters, which are in contact with the clay core. The gases dissolved in the water diffuse towards the vessel on the opposing side, where its concentration is lower. Once the experiment has started, sampling must be done on a regular basis. Generally, this means in the beginning once a week and later in the experiment the frequency can be increased until around 10 data points, in a linear region, are obtained. The gas composition is analyzed with gas chromatography, using the Compact GC 4.0. The experiment is carried out in a temperature controlled room of 21 ± 2 °C (Jacops et al., 2013).

5.2.3 Diffusion transport model

The diffusion transport model in a 1D geometry represents the diffusion equation based on the first and second law of Fick.

$$F = -\eta D_p \frac{\delta c}{\delta x} \tag{4}$$

$$\frac{\delta c}{\delta t} = D_{app} \frac{\delta^2 c}{\delta x^2} \tag{5}$$

In these equations, F is the flux in mol/s·m^2, η stands for the porosity (-), D_p is the pore diffusion coefficient expressed in m^2/s, c denotes the concentration in the porous medium expressed in mol/m^3, t is the time in s, x is the length in m, and D_{app} denotes the apparent diffusion coefficient in m^2/s.

There is a relationship between the pore diffusion coefficient, the apparent diffusion coefficient, and the effective diffusion coefficients, expressed in equation 6.

$$D_{app} = \frac{D_p}{R} = \frac{D_{eff}}{\eta R} \tag{6}$$

With R the retardation factor and ηR the capacity factor, which is the product of the retardation factor and the porosity. Considering no significant interaction between the dissolved gases and the sample, meaning no adsorption, the retardation factor equals 1.

The results of the diffusion experiments are modeled by fitting the solutions of the diffusion equation with proper initial conditions and boundary conditions. For gas diffusion experiments, the parameters that can be obtained are the D_{app} and the capacity factor ηR. However, in the case of fast gas diffusion experiments, ηR is set constant with an average value found in literature from Bruggeman et al. (2009) and only D_{app} is fitted since both parameters are correlated. The decrease of the inlet pressure at both sides as a result of sampling needs to be taken into account as a boundary condition.

The diffusion equation is solved by COMSOL Multiphysics coupled with MATLAB. COMSOL Multipysics is a finite element-based analysis, solver, and multiphysics simulation software, which is used for various applications in engineering and physics. Subsequently, the diffusion coefficient is obtained by using a least square fitting procedure to the obtained experimental results with the MATLAB Optimization Toolbox. The Levenberg-Marquardt method is used by the Toolbox on a Trust region, which is preferably as small as possible to optimize the result of the least square problem.

5.3 Characterization of the samples

5.3.1 Chemical Analysis

X-ray Diffraction

XRD is an analytical technique used for phase identification of crystalline material. The working principle of XRD is based on the constructive interference of X-rays that are reflected by the atom planes. In the X-ray tube, electrons are accelerated by applying a voltage, toward a target. The electrons bombarding the target lead to the excitement of the inner shell electrons, and the produced vacancies are subsequently filled by outer shell electrons. When the outer shell electrons fill the vacancies, characteristic X-rays are produced and emitted towards the analyzed sample. Parallel X-rays hit the sample under an exact incident angle θ and the reflected or 'diffracted' rays will interfere constructively and the X-rays will be detected. According to Bragg's law,

$$2d \sin\theta = n\lambda \tag{7}$$

the difference between 2 scattered X-rays is d and the pair-length difference $2dsin\theta$ is a multiple of the wavelength λ.

For XRD-analysis, the sample needs to be dried and milled in order to have a fine, homogenized particle distribution. Next, the sample is packed into the XRD sample holder with a side-loading technique. The measurements were performed at SCK-CEN with a Bruker D8 Advance with LynxEye detector, Cu-bron, and Kβ filter, and primary and secondary soller slits of 2.5°.

5.3.2 Petrophysics

Porosity measurement by drying

The porosity is measured after the double-through diffusion experiment by the weight difference of the sample before and after the dry oven at a temperature of 105°C. After the experiment, the sample is considered saturated and a subsample of ± 20g is taken, subsequently, the weight is registered on a regular base until its stable.

The porosity η can be calculated by the following equation (Aertsens et al., 2012).

$$\eta = \frac{(m_{wet} - m_{dry})\rho_{sol}}{m_{dry}\rho_{liq}} + (m_{wet} - m_{dry})\rho_{sol} \tag{8}$$

N_2-adsorption

The nitrogen adsorption method measures the available pore volume and the specific surface of the samples. At SCK-CEN the Micromeritics Instrument TriStar II 3020 V1.03 (V1.03) is used. The samples need to be dried and milled, next, they are filled in a sample tube and degassed at room temperature for 30 minutes at 110 °C for 24 hours. Subsequently, the sample tube is packed in an isothermal jacket and put in a dewar flask which is filled with liquid N_2. The Micromeritics Instrument measures the amount of gas that is adsorbed on the sample as a function of the relative pressure and a sorption isotherm is obtained. Next, the specific surface area (SSA) of the sample is calculated by using the Brunauer, Emmet and Teller (BET) theory. The BET-equation gives the relations between the number of adsorbed gas molecules (X) at a given relative pressure (P/P_0) (Lowell et al., 2006).

$$\frac{1}{X((P_0/P)-1)} = \frac{1}{X_{N_2}C} + \frac{C-1}{X_{N_2}C}(\frac{P}{P_0}) \tag{9}$$

The adsorption isotherm can be plotted based on the BET-equation, resulting in a linear plot of $1/X((P_0/P)-1)$ in function of P/P_0. The surface area is then calculated from the slope and intercept according to following equation.

$$SA = \frac{1}{slope + intercept} * A \tag{10}$$

With A being the cross-sectional area of the adsorbate N_2 (Thommes et al., 2015).

Low pressure, between 0 – 0.2 P/P_0, provides adsorption on a first layer on the external surfaces and filling of nanopores smaller than 4 nm. Higher relative pressure confers adsorption on the second and third layers and the mesopores between 4 and 40 nm are filled. At last, when the relative pressure exceeds, condensation in the macropores, larger than 40 nm, occurs (Bergaya & Lagaly, 2013).

Nuclear Magnetic Resonance Spectroscopy

NMR is an advanced characterization technique, which is used to determine the properties of fluid-saturated porous rocks. The technique for this particular purpose is based on nuclear spin relaxation. The signal produced from hydrogen nuclei is proportional to the concentration of the H-atoms in the sample and allows to determine many important characteristics as porosity, pore size distribution, permeability, and water saturation. Different relaxation times are expected for the induced excited energy states of hydrogen-containing molecules in different regions. The relaxation time for a molecule close to the surface is

much shorter, compared to a molecule in the bulk volume. The difference is a consequence of paramagnetic centers in the pore wall surface and the calculations are based on two relaxation times, longitudinal T1 and transverse T2 relaxation time (Dunn et al., 2002). The transverse relaxation experiment is the most valuable source of information for petrophysical characterization in an NMR measurement (Testamanti & Rezaee, 2017).

Cation exchange capacity

For the CEC measurements, the samples have been dried in a dry oven at 105C. Next, the sample is mixed with an exchange solution which consists 0.01 M Cu(II)-triethylenetetramine, also known as Cu-trien, and distilled water. Calcite is added to the solution to prevent the dissolution of carbonates in the Boom Clay or Eigenbilzen Sand (Frederickx et al., 2018). This mixture is subsequently placed in an ultrasonic bath for 30 minutes and then stirred for 30 minutes. In the centrifugation tubes, 1 to 3 g of the sample is mixed with 50 ml of the solution. The tubes are centrifuged in a horizontal shaker for 24 hours and the supernatant is separated by centrifugation. To determine the cation exchange capacity, the concentration of Cu^{2+} complex in the solution is obtained with UV-VIS spectrophotometry by measuring the extinction of the solution at 577nm. The CEC is calculated as the difference between Cu-trien initially added and Cu-trien which was not adsorbed on the sample and therefore still in the solution. To have a second calculation of the CEC and to obtain the concentration of the exchangeable cations, ICP analysis is executed. Due to the percolation of the samples with $NaNO_3$, also NO_3 is measured with ICP so a distinction can be made between Na^+ adsorbed on the clay surface and Na^+ in the pore volumes as $NaNO_3$.

6 Results and discussion

6.1 Impact of $NaNO_3$ on the hydraulic conductivity

One of the most important transport properties is the hydraulic conductivity (K) as it is a measure of how easily water can pass through a porous material. The K-value depends on the pore size and the pore connectivity and is low for materials with low porosity and narrow pore throats. For geological disposal of radioactive waste, a low hydraulic conductivity is crucial to minimize the pressure-driven migration of water potentially contaminated with radionuclides. Using Darcy's law the K-value of the percolated Boom Clay and Eigenbilzen Sand is calculated for a 1 M $NaNO_3$ water solution and the K-value for the non-perturbed Eigenbilzen Sand with synthetic pore water of 0.014 M $NaHCO_3$. The results of these tests are shown in Table 1.

Table 1: Hydraulic conductivity of all the analysed samples and the reference samples.

Sample Origin	Sample Name	Orientation	K_{eff} (m/s)
Boom Clay	NaNi H4-disturbed	//	$2.2 \pm 0.03 \times 10^{-12}$
Boom Clay	NaNi H4-undisturbed	//	$3.5 \pm 0.07 \times 10^{-12}$
Boom Clay	K4	//	$3.4 \pm 0.04 \times 10^{-12}$
Eigenbilzen Sand	Mol2A-disturbed	⊥	$5.2 \pm 2.00 \times 10^{-10}$
Eigenbilzen Sand	Mol2A-undisturbed	⊥	$3.4 \pm 0.70 \times 10^{-10}$
Eigenbilzen Sand	K17	⊥	$4.2 \pm 0.20 \times 10^{-10}$

The reference value for Boom Clay is the sample 'K4' and the reference value for Eigenbilzen Sand is the sample 'K17', both from the paper of Jacops, Aertsens, Maes, Bruggeman, Krooss, et al. (2017). The reference samples are rather well comparable to the analysed samples of this study. The Boom Clay reference K4 originates, just like NaNi H4, from the Putte and Terhaegen Member and is oriented parallel to the bedding. The reference K17 is an Eigenbilzen Sand formation sample and is oriented perpendicular to the bedding. Since clay formations are anisotropic, it is important that the reference sample has the same orientation as this has an influence on the hydraulic conductivity. In horizontal cores, parallel to the bedding, the hydraulic conductivity is higher than in vertical cores. This is a result of the alignment of the flat mineral surfaces in horizontal direction.

The hydraulic conductivity of NaNi H4 was also measured in 1999, at the start of the Long Term Experiment, when the sample was not yet perturbed by $NaNO_3$ (Bleyen et al., 2018). Therefore a direct comparison can be made between the disturbed and undisturbed NaNi H4 sample. Since there 2 samples of Mol2A-189, disturbed and undisturbed, also for Eigenbilzen Sand a direct comparison is possible. The impact of $NaNO_3$ on the hydraulic conductivity of Boom Clay or Eigenbilzen is imperceptible. There is a slight difference in value, but this variation is not enough to perceive it as a consequence of the $NaNO_3$ percolation. It seems that advective transport is not influenced by the geochemical perturbation.

6.2 Diffusion experiment

The detailed measurements of each sampling moment, including the logbook, can be found in ANNEX. For the perturbed Boom Clay, labeled as 'NaNi', 11 data points were obtained in a period of 67 days. The experimental data of the dissolved gases are fitted based on the concentration of the outlet concentration. To fit the apparent diffusion coefficient, an average value of 38% is used as porosity. After further characterization techniques, the porosity is calculated for NaNi, however, the porosity has not changed so the diffusion coefficients do not need to be recalculated.

Figure 9 shows the graphs of the experimental data and the model fit. The model gives a lower R^2 for methane CH_4 than for the other gases. Therefore, a correction has been done by eliminating the first days and subtracting the background of 300 ppm of the first measurement point from all the other samples. The enriched background could possibly be a side effect of contamination of the vessel. The new corrected model has an improved fit on the measured data, as can be seen in Figure 9.E. The correction has been done because the model is not suited to work with a background (¿ 0 ppm) and the first days are eliminated because of the detection limit of CH_4.

The other 3 gases do not need a correction as the model nicely fits the experimental data. Although, for the gases C_2H_6 and Xe, which are measured together since they are in the same water vessel, the 4th data point is considered as outlier. The concentration of this 4th measurement is too high, in comparison to the third and fifth data points. The increased concentration is probably due to contamination of the sampler, which could happen if the sampler is not flushed thoroughly enough.

The experimental results and the fitted model of the percolated Eigenbilzen Sand, labeled

as 'Mol2A-disturbed', are shown in Figure 10. The diffusion experiment is accomplished in 39 days and 10 data points were acquired during this period.

The gases C_2H_6 and Xe, which are both in the same vessel, start immediately with a very high concentration, as a possible effect of contamination of the low-concentration compartment. Considering only the net-outflux is necessary to calculate the diffusion coefficient, the data is corrected by a net concentration decrease of 700 ppm for C_2H_6 and 1300 ppm for Xe. After this adjustment, the experimental data starts from zero and the model fits the data with a small variance. Same remark as above, the model cannot compute with a background, so the only solution is to correct by subtracting the background manually. It is possible that the concentration was increased by external contamination of the samples. It could also be a result caused by a little crack in the sample, through which the gases have found a pathway. However, if this would be the case, the diffusion coefficient of the gases should be higher than expected and this is not the case, as explained below in Chapter 6.3.

The two other gases He and CH_4 start with a delay in time, so a zero concentration for the first two sampling points. Correction is accomplished by removing the first days and deleting the two zero concentration points, this results in a much better fit. This correction is justified since measurements of low concentration are not very reliable. Especially for CH_4, which has a lower limit of 100 ppm for reliable peak detection.

The results of the last diffusion experiment, from the undisturbed Mol2A, are given in Figure 11. Since the diffusion experiment only could be set up on 19/04/2022, there was a bit of a time crunch to end the experiment on time. Therefore, there are only 7 data points available over a period of 22 days. However, considering the 7 data points fall in the linear region and the diffusion coefficient is calculated based on the flux over this linear region, the results are considered accurate enough.

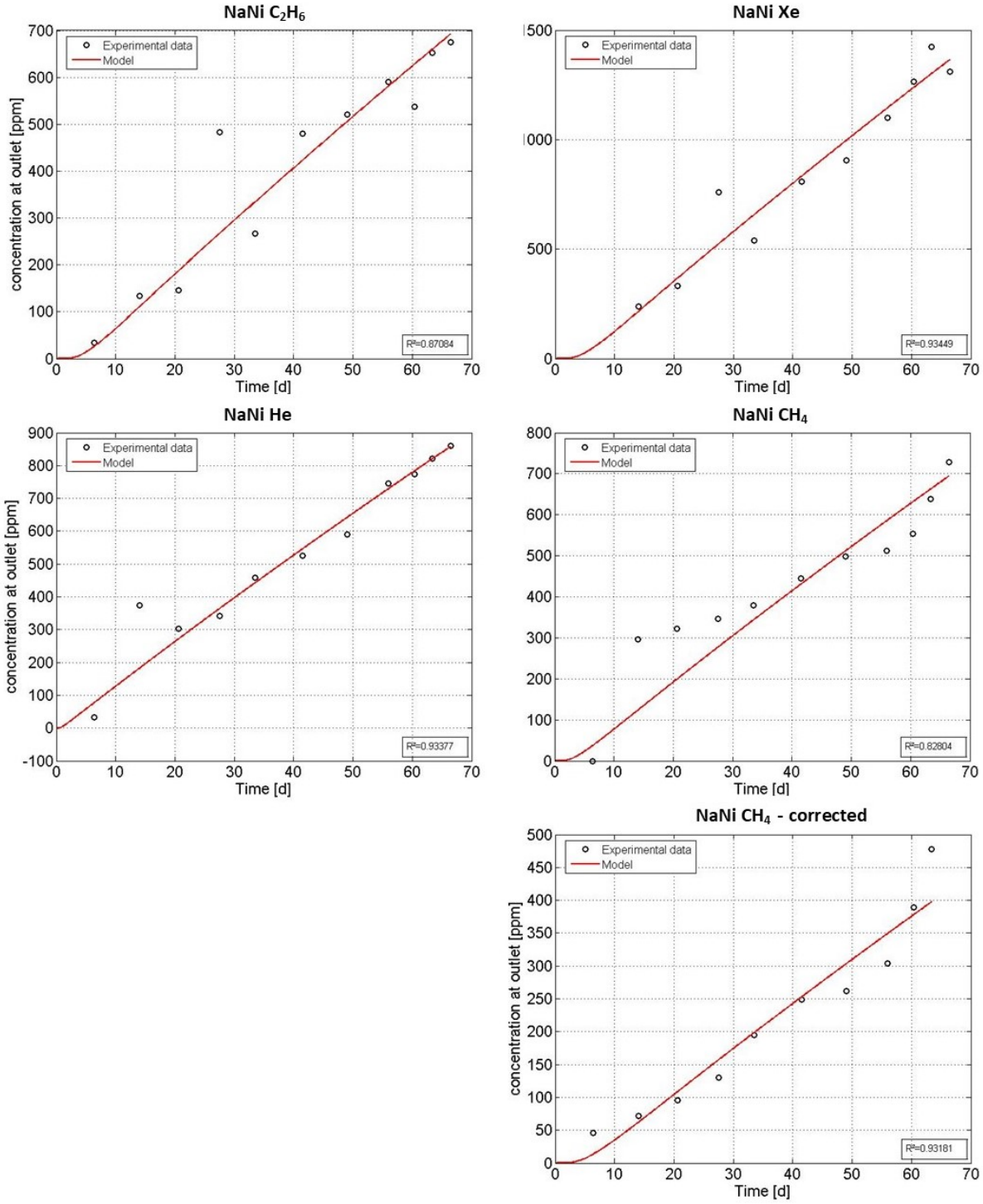

Figure 9: Double-through diffusion experiment of the disturbed Boom Clay, NaNi H4. The 4 dissolved gases, C_2H_6, Xe, He, CH_4, are fitted based on outlet concentration in function of time.

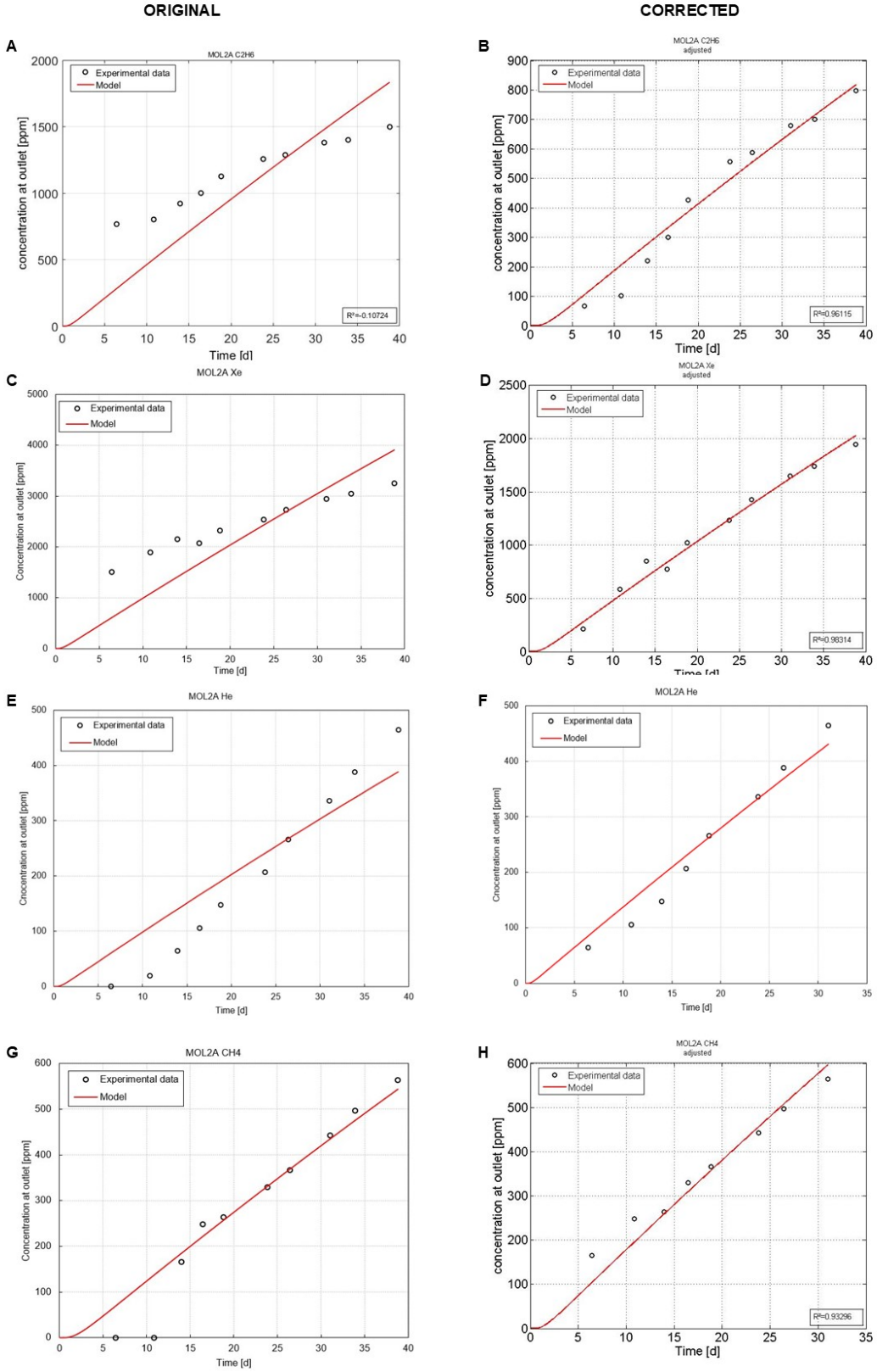

Figure 10: Double-through diffusion experiment of the disturbed Eigenbilzen Sand, Mol2A-189. The 4 dissolved gases fitted based on outlet concentration in function of time. A) C_2H_6 B) corrected C_2H_6 C) Xe D) corrected Xe E) He F) corrected He G) CH_4 H) corrected CH_4

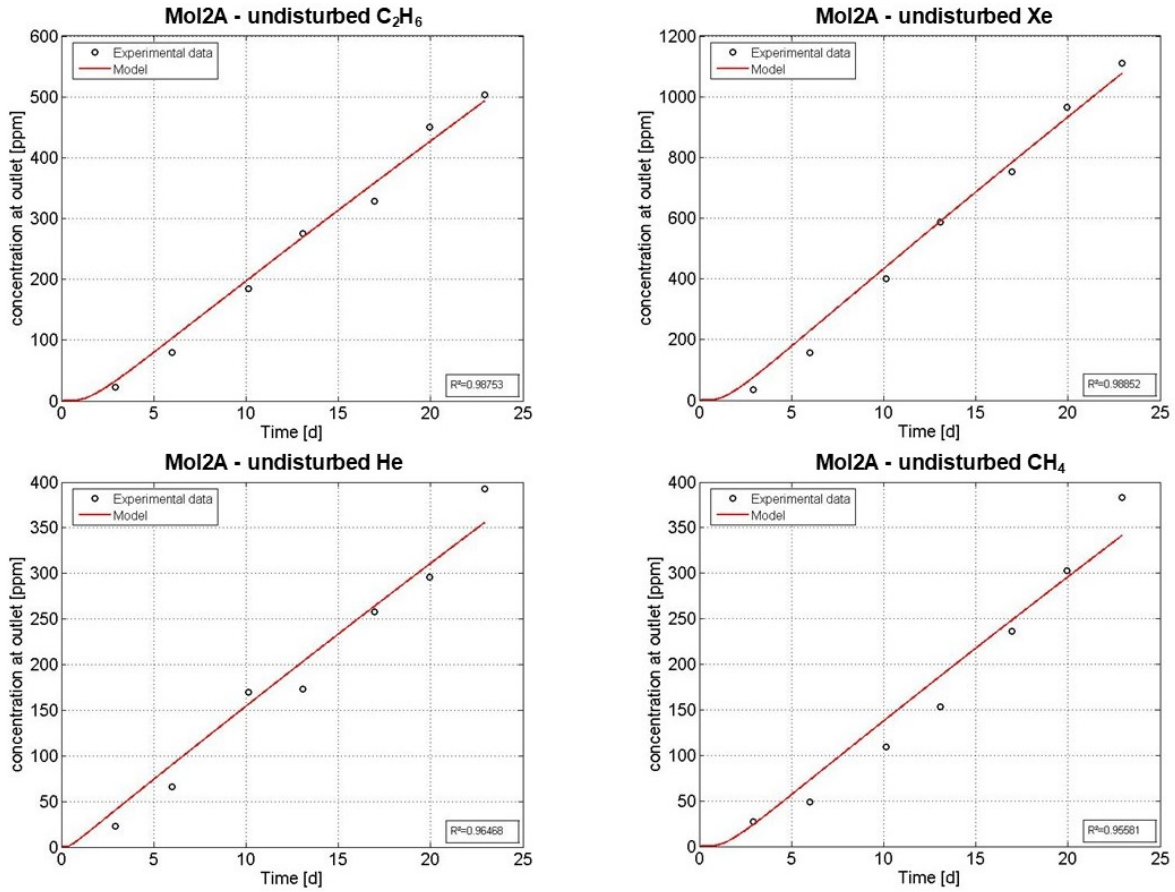

Figure 11: Double-through diffusion experiment of the undisturbed Eigenbilzen Sand, Mol2A-189, with 4 dissolved gases fitted based on outlet concentration in function of time.

6.3 Impact of $NaNO_3$ on the diffusion coefficient

As discussed in Chapter 4, the ionic strength of the clay is increased by the presence of $NaNO_3$ and could have an influence on the transport properties. To assess the effect, experiments are performed by percolating Boom Clay and Eigenbilzen Sand and comparing D_{eff} of the chemically disturbed samples with D_{eff} of the undisturbed samples NaNi H4 from Bleyen et al. (2018), Mol2A-189 and the reference samples K4 and K17 from Jacops et al. (2017).

In Table 2, the values of the 4 gases, which were used in the double-through diffusion experiment, are listed. Their uncertainty is determined from a 95% confidence interval by the diffusion model. In Figure 12, the values are represented in a bar chart, to make a visual comparison. The D_{eff} of tritiated water (HTO), a radioactive form of water, is plotted on the bar chart as well. HTO was calculated in disturbed and undisturbed NaNi

H4 in the Long Term Experiment in Bleyen et al. (2018) and in the undisturbed K4 in Jacops et al. (2017).

HTO is studied for undisturbed NaNi H4 and undisturbed K4, so a comparison between the two samples will indicate whether K4 is a good reference for NaNi H4. It appears from Figure 12 that the D_{eff} of HTO in both samples is very similar. Accordingly, using K4 as a reference undisturbed sample to compare with the disturbed NaNi H4 sample is acceptable. The same reasoning is applied for undisturbed Mol2A-189 and K17, except there is no data available of HTO. The diffusion coefficients of the gases in both samples seem to correspond rather well, confirming that K17 is a good reference. However, it is still more interesting to compare the disturbed Mol2A-189 to the undisturbed Mol2A-189 as this is the exact same sample and therefore more representative.

From Figure 12, there is a subtle trend visible, namely that the D_{eff} of the undisturbed sample is generally higher than the D_{eff} of the disturbed sample for every gas and HTO. However, Bleyen et al. (2018) concluded that the diffusion coefficient of HTO was not affected by geochemical perturbation due to $NaNO_3$, as the difference between the D_{eff} is too small to be considered. It is true that the difference between disturbed and undisturbed is limited, nevertheless, this small decrease is perceptible in every gas.

Cautiously, the conclusion can be made that perturbation due to $NaNO_3$ leads to a modest decrease in the effective diffusion coefficient. According to Jacops et al. (2020), K is strongly correlated to D_{eff} for Boom Clay and Eigenbilzen Sand. This is however not observed in these results, as K is considered constant after perturbation and D_{eff} decreases. It proves that advective transport is not similarly affected as diffusive transport and that geochemical perturbation only has an impact on diffusive transport.

From Figure 12, it is also apparent that the diffusion coefficient of the gases in the Boom Clay is lower than in Eigenbilzen Sand, although both formations have a similar porosity. This is denoted to the lower permeability (advective transport) of Boom Clay and thus a lower accessible pathway for the gases.

To summarize, advective transport has an influence on diffusive transport, as a lower permeability is linked to a lower diffusion coefficient. However, advective transport is less affected by perturbation, as the permeability does not decrease for Boom Clay and Eigenbilzen Sand and the diffusion coefficient of the smallest gases does.
The ratios of the diffusion coefficients from the chemically disturbed over the undisturbed

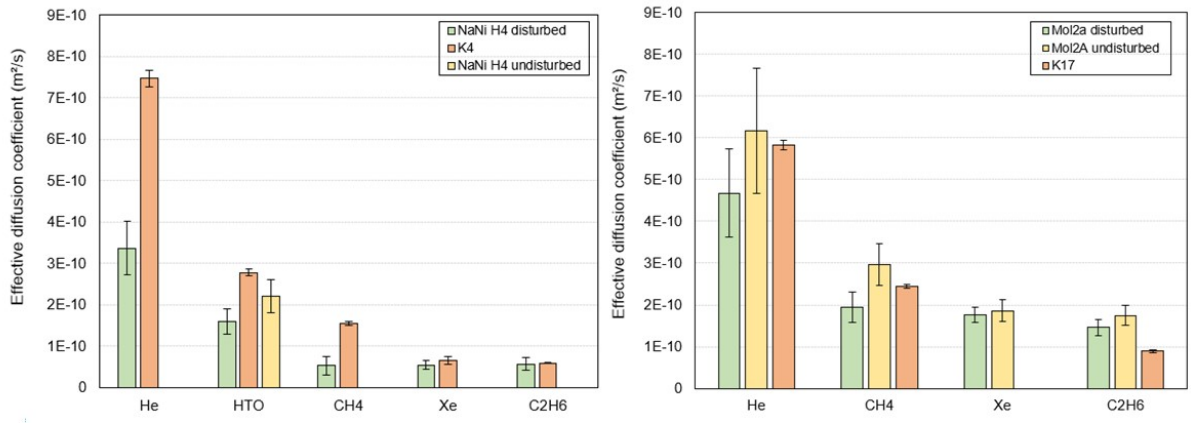

Figure 12: The calculated effective diffusion coefficient of the dissolved gases He, CH_4, Xe and C_2H_6, and HTO (Bleyen et al., 2018) from the disturbed Boom Clay (left) and Eigenbilzen Sand (right), are plotted in green. These are compared to D_{eff} of K4 and K17 from Jacops et al. (2017), plotted in orange, and compared to D_{eff} of the undisturbed Boom Clay and Eigenbilzen Sand, plotted in yellow.

samples are presented in Figure 13. The undisturbed sample for Boom Clay is K4 and for Eigenbilzen Sand is undisturbed Mol2A-189. How lower the bar chart, how more impact $NaNO_3$ has on the diffusion coefficient. Boom Clay is illustrated on the right and in particular the gases He and CH_4 are remarkably affected by $NaNO_3$, they have a reduced diffusion coefficient in comparison to the undisturbed Boom Clay. HTO is also plotted in Figure 13 on the right, to visualize that HTO follows the trend of a minor diffusion coefficient decrease after perturbation. On the left, Eigenbilzen Sand is shown and the ratios are much closer to 1. Eigenbilzen Sand has fewer clay minerals and is therefore also expected to be less impacted by $NaNO_3$.

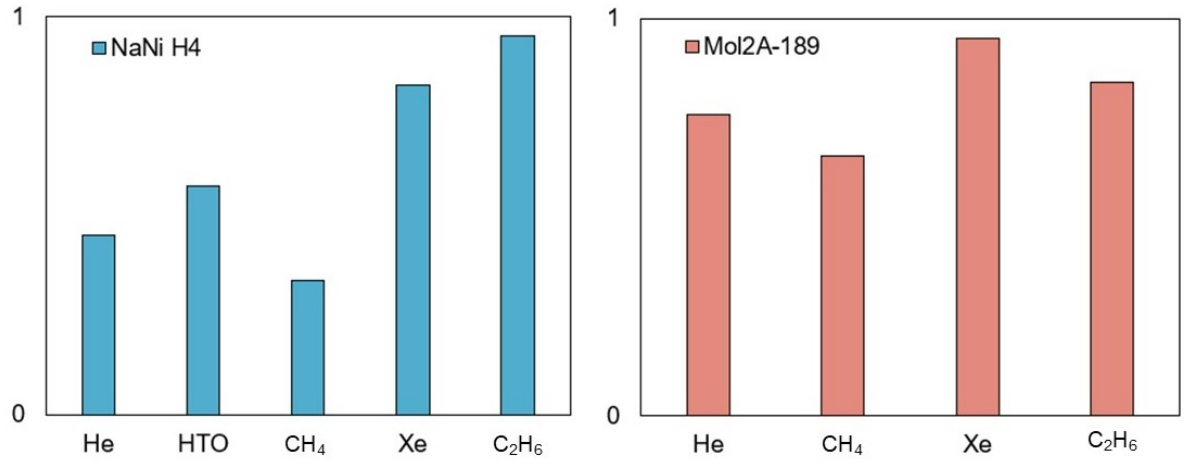

Figure 13: Ratio of the effective diffusion coefficient from the disturbed sample over the undisturbed sample of Boom Clay (left) and Eigenbilzen Sand (right).

The size of the diffusing molecules is represented by the kinetic diameter (σ) (Matteucci et al., 2006). There are two different calculations to obtain the kinetic diameter, one is by second virial coefficients and is better suited for thermodynamic properties and calculations and the other is by viscosity measurements and is more appropriate for transport property calculations. Therefore, the kinetic diameter obtained by viscosity measurements is given in Table 2, taken from Hirschfeld et al. (1954). These kinetic diameters are representative for a dilute gas mixture and are therefore only approximations of the size of dissolved gases in solution (Jacops, Aertsens, Maes, Bruggeman, Swennen, et al., 2017).

For Boom Clay, the D_{eff} of all the gases and HTO in NaNi H4 and in K4 in function of the size of diffusing molecule is illustrated in Figure 14. It is explained above, why K4 is an appropriate reference Boom Clay sample. In addition, in Figure 14, the D_{eff} of additional undisturbed Boom Clay samples are plotted as well, to have more than 1 reference sample. Since these additional undisturbed Boom Clay samples have a perpendicular orientation, the anisotropy factor of 1.5 is applied to make a representative comparison (Jacops et al., 2017). All the diffusion coefficients of the undisturbed Boom Clay samples are very much alike after correction. The D_{eff} of the gases in function of kinetic diameter for Eigenbilzen Sand is shown in Figure 15.

The diffusion coefficient clearly decreases with an increase in the kinetic diameter. The trend line for the dependence of D_{eff} on the kinetic diameter is expressed by following equation (Jacops et al., 2017):

$$D_{eff} = D_{eff,exp} \times exp(-n_{exp}\sigma) \tag{11}$$

The exponential factors n_{exp} of disturbed NaNi H4 and K4 are subtly different, they are respectively 9.52×10^9 and 12.3×10^9 As well as the n_{exp} of Mol2A-disturbed, Mol2A-undisturbed and K17, which are respectively 6.43×10^9 , 7.13×10^9 and 9.73×10^9 , have a very subtle difference. Hence, the relation between the diffusion coefficient and the diffusing molecule size is to some extent alternated by $NaNO_3$ as the trend line is less steep for the disturbed samples. This difference will also be observed in a change of the geometric factor, which will be explained in Chapter 6.4 below.

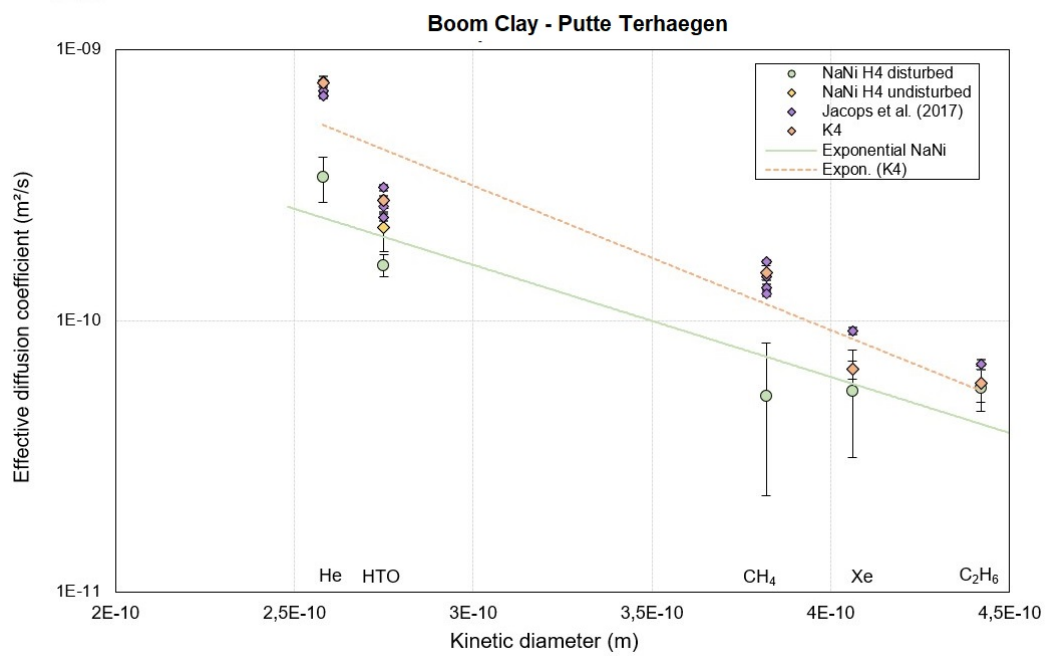

Figure 14: Boom Clay: Effective diffusion coefficient in function of the kinetic diameter. Disturbed NaNi H4 in green, undisturbed NaNi H4 in yellow, undisturbed reference sample K4 from Jacops et al. (2017) in orange and additional reference samples from Jacops et al. (2017) in purple.

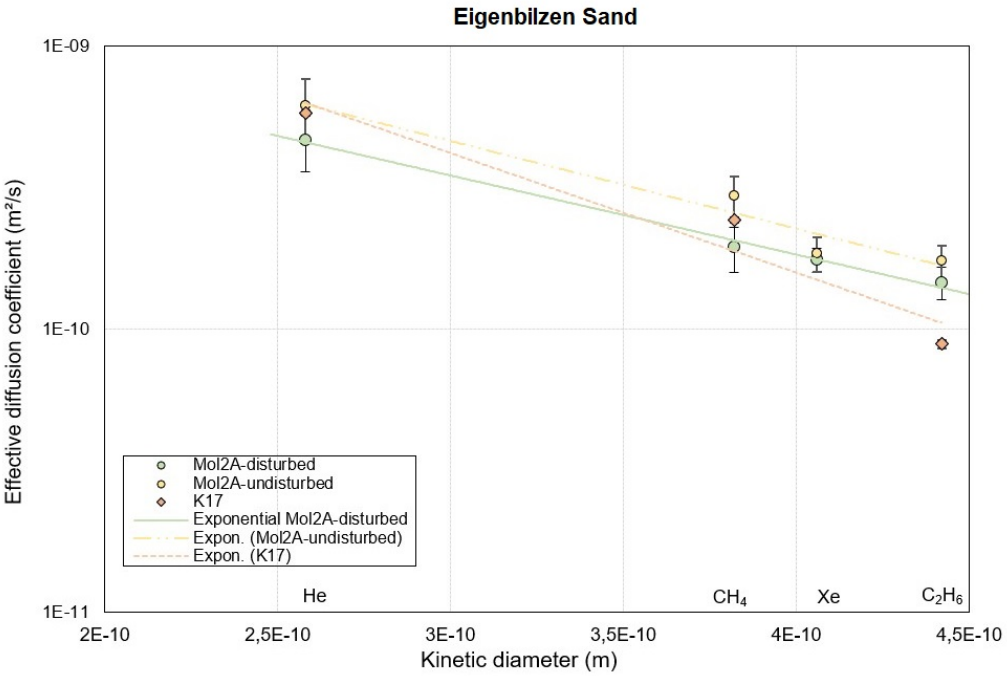

Figure 15: Eigenbilzen Sand: Effective diffusion coefficient in function of the kinetic diameter. Disturbed Mol2A-189 in green, undisturbed Mol2A-189 in yellow and undisturbed reference sample K17 from Jacops et al. (2017) in orange.

6.4 Impact of $NaNO_3$ on the geometric factor

The geometric factor gives the relation between the diffusion coefficient in a porous medium (D_{eff}) and the diffusion coefficient in water (D_0):

$$G = \eta \frac{D_0}{D_{eff}} \tag{12}$$

D_{eff} is retrieved from the diffusion experiment and D_0 is taken from Boudreau (1996), given in Table 2.

Another expression for the geometric factor, used in the study of Grathwohl (1998) is as follows:

$$G = \frac{\tau}{\delta} \tag{13}$$

With τ the tortuosity and δ the constrictivity. The tortuosity is a dimensionless parameter and is known as the ratio of the effective length of the path of the diffusing molecule to the shortest distance of this path (Bini et al., 2019). Constrictivity is also a dimensionless parameter, significant in transport processes. It considers the reduction of D_{eff} as a result of the friction with the pore wall, hence depending on the ratio of the diameter of the molecule to the pore size distribution.

Constricitivity can be calculated with the empirical expression of Grathwohl (1998):

$$\delta = exp(-4.6\frac{\sigma}{R_{\text{pore}}}) \tag{14}$$

σ is the kinetic diameter in meter and R_{pore} is the pore width in meter as well. This is an approximation as the simplification is made that there is only one pore size, however, in reality, clay has a pore distribution. For large pores, δ equals 1 and becomes smaller and therefore more important if the size of the diffusing molecule is similar to the pore diameter (Bini et al., 2019).

By substitution, the new formula for the geometric factor becomes:

$$G = \tau \cdot exp(4.6\frac{\sigma}{R_{\text{pore}}}) \tag{15}$$

So the geometric factor relates the size of the diffusing molecule σ and the pore size R_{pore} and G should increase in function of σ. If the exponential factor is approximated by one, the geometric factor remains constant, this occurs when σ is sufficiently small, with respect to R_{pore}. For an increase in size of the diffusing molecule, fewer pores will be

accessible for transport by diffusion of the molecule. Initially, the path length (τ) will become longer as only pores larger than the size of the diffusing molecule are accessible. With a further increase in the size of the molecule, there will no longer be a connected path for diffusion, so D_{eff} becomes zero.

The geometric factor in Table 2 is calculated with Equation 12, with data from the diffusion experiment for D_{eff}. In Figure 16, the geometric factor of the Boom Clay samples is plotted against the kinetic diameter. Based on the graph, it seems that there is a slight increase of G with increasing σ for the undisturbed as for the disturbed samples. However, the range of increase is so small-scaled if compared to other types of clays as Bentonite Clay, see figure 18. The geometric factor of Bentonite Clay increases steeply with a factor of 16, due to the small R_{pore}, with a similar size as the molecule. Because when the size of the diffusing molecule is large in comparison to the pore size, R_{pore} becomes more important and the pore throats will establish if gas can pass through the pore network without difficulty. As Boom Clay has larger pores the increase of G is less prominent (Jacops et al., 2017). As explained above, this is solely an approximation due to the simplification of neglecting the pore size distribution.

Another remark based on the graph of Boom Clay, G seems to be larger for all the gases of the disturbed NaNi H4 than for the undisturbed K4. The increase of G after perturbation corresponds to the decrease of D_{eff}. In particular the smaller molecule He is affected by $NaNO_3$, with an increased G in comparison to the undisturbed.

HTO data from Bleyen et al. (2018) and Jacops et al. (2017) is also plotted in the Figure 16, to study the difference in geometric factor between disturbed and undisturbed Boom Clay sample. Also for HTO, G seems to enlarge slightly after percolation of $NaNO_3$.

In Figure 17, the geometric factors of the Eigenbilzen Sand samples is plotted. Due to the very small range in comparison to Bentonite Clay in Figure 18, G is considered constant for the Eigenbilzen Sand samples. The pore size is large enough with respect to the kinetic diameter of the gases, causing the exponential factor to be approximated by one.

Table 2: The kinetic diameter (σ) and diffusion coefficient in free water (D_0) of the gases and HTO, the measured effective diffusion coefficient (D_{eff}) of the dissolved gases and HTO in disturbed and undisturbed NaNi H4 and Mol2A-189 and their geometric factor (G). NA = Not Available

			Boom Clay				Eigenbilzen Sand			
	σ (m) x 10^{-10}	**D_0 (m^2/s) x 10^{-9}**	**D_{eff} (m^2/s) x 10^{-10}**			**G (-)**	**D_{eff} (m^2/s) x 10^{-10}**			**G (-)**
			NaNi H4 Disturbed	*NaNi H4 Undisturbed*	*K4*		*Mol2A Disturbed*	*Mol2A Undisturbed*	*K17*	
He	2.58	7.30	3.37 ± 0.65	NA	7.47 ± 0.2	8.24	4.68 ± 1.06	6,16 ± 1.5	5.82 ± 0.11	5.90
HTO	2.75	2.20	1.6 ± 0.30	2.20 ± 0.4	2.78 ± 0.09	5.23	NA	NA	2.99 ± 0.27	NA
CH_4	3.82	1.80	0.52 ± 0.12	NA	1.55 ± 0.05	13.0	1.95 ± 0.36	2.97 ± 0.51	2.44 ± 0.05	3.50
Xe	4.06	1.50	0.55 ± 0.10	NA	0.66 ± 0.09	10.4	1.77 ± 0.81	1.86 ± 0.26	NA	3.21
C_2H_6	4.42	1.40	0.56 ± 0.15	NA	0.59 ± 0.01	9.45	1.46 ± 0.19	1.74 ± 0.24	0.89 ± 0.03	3.61

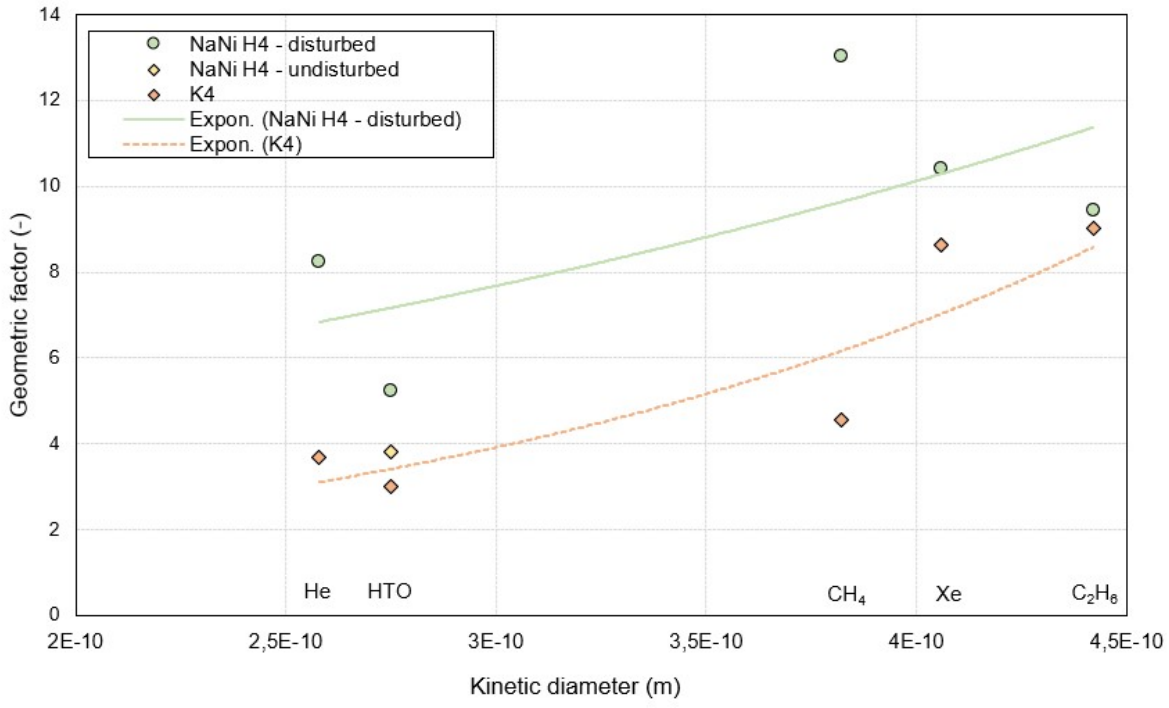

Figure 16: Geometric factor of Boom Clay in function of the kinetic diameter. The dissolved gases and HTO of the disturbed NaNi H4 sample are plotted in green, HTO of the undisturbed NaNi H4 sample from Bleyen et al. (2018) is plotted in yellow, the dissolved gases and HTO of the undisturbed reference sample K4 from Jacops et al. (2018) are plotted in orange.

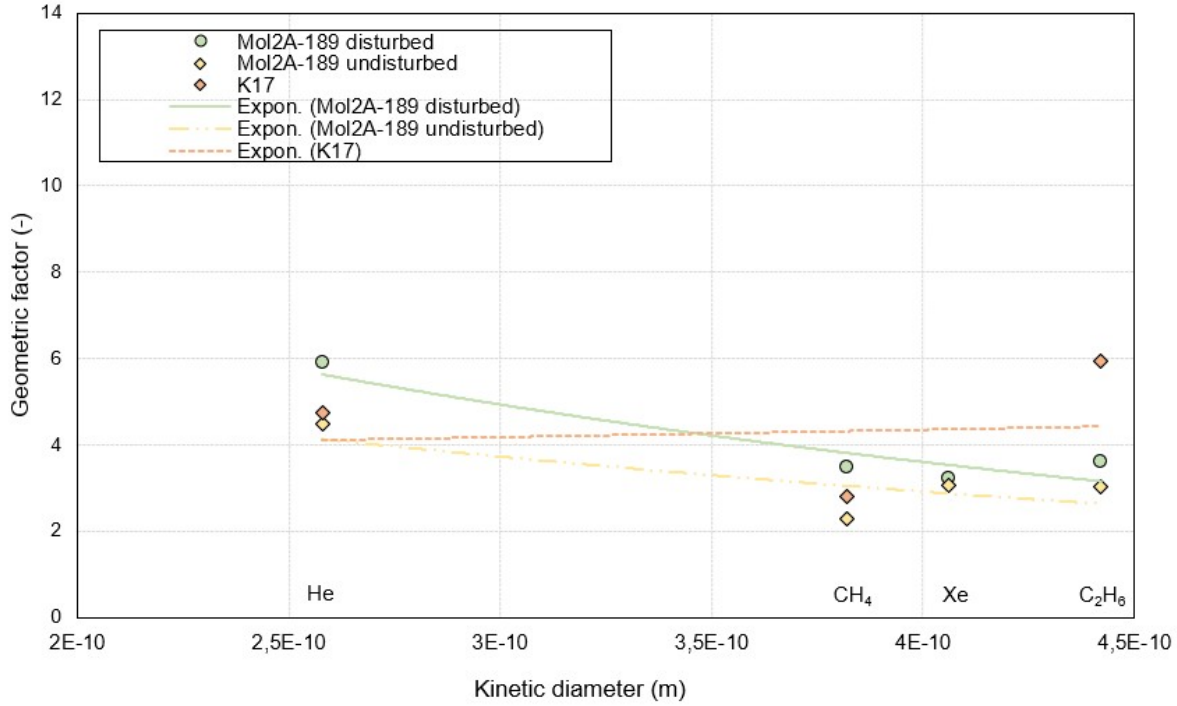

Figure 17: Geometric factor of Eigenbilzen Sand in function of the kinetic diameter. The dissolved gases of the disturbed Mol2A-189 sample are plotted in green, the dissolved gases of the undisturbed Mol2A-189 sample are plotted in yellow, the dissolved gases of the undisturbed reference sample K17 from Jacops et al. (2018) are plotted in orange.

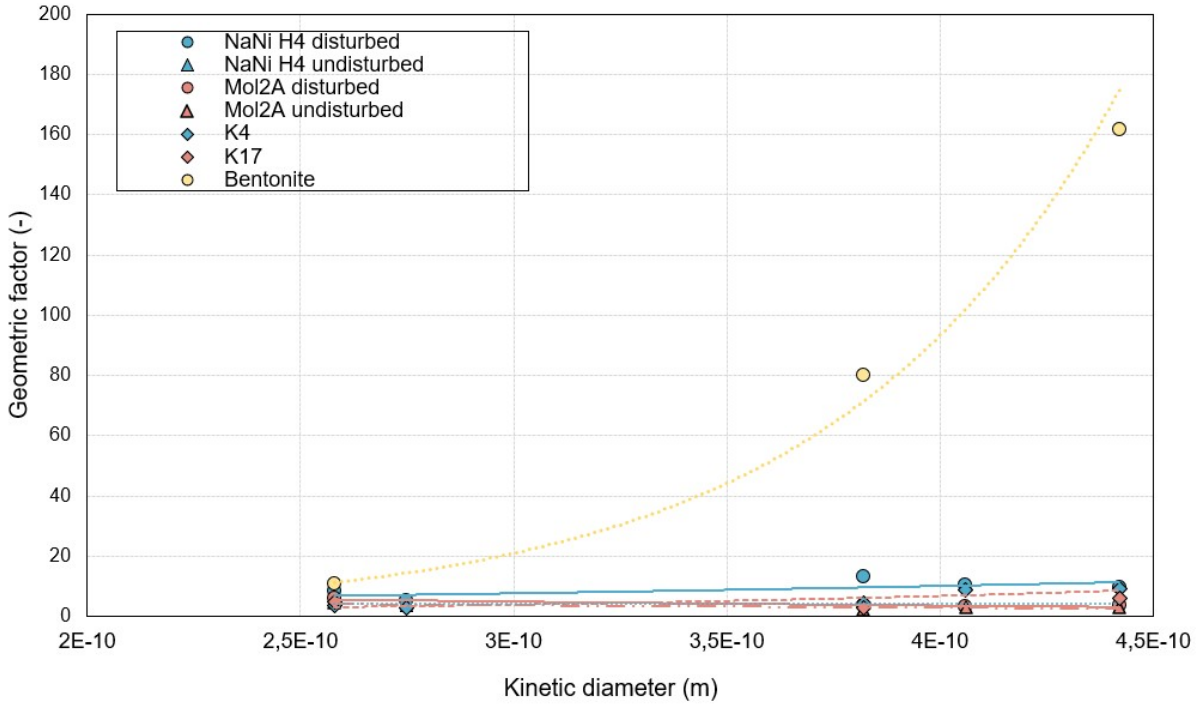

Figure 18: Geometric factor of Boom Clay, Eigenbilzen Sand and Bentonite Clay, with data from Jacops et al. (2017).

6.5 Impact of $NaNO_3$ on the mineralogy and the specific area

In Table 3, the mineralogical composition obtained by XRD analysis is given. Boom Clay and Eigenbilzen Sand are both mainly dominated by quartz and 2:1 clay-minerals. The sample of percolated Boom Clay, NaNi H4, consists of 16% quartz and 66% 2:1 clay minerals. These 2:1 clay minerals include the illite, smectite, illite-smectite mixture, and muscovite layers.

Without a detailed analysis, it is hard to quantify the smectite concentration. Although, an estimation of the smectite weight percentage can be made, relying on the data of Frederickx et al. (2018):

$$log(\frac{Smectite(wt\% < 0.2\mu m)}{\sum ClayMinerals(< 0.2\mu m)}) = -0.73log(\sum ClayMinerals((bulk)) + 0.89 \quad (16)$$

The predicted wt% of smectite layers in the case of NaNi is 26 wt%. The attained percentages of quartz and clay fall in the foreseen range of Boom Clay for the Putte-Terhaegen Member, from which NaNi H4 originates. The Putte-Terhaegen Member has the lowest quartz content and is the most clay-enriched, compared to all the other Members of the Boom Clay (Frederickx et al., 2021). Although in comparison to the reference sample K4 of Jacops et al. (2017), NaNi H4 is even more clay-enriched, as K4 has a quartz content of 28% and a 2:1 clay mineral content of 49%.

As expected, the undisturbed and disturbed Eigenbilzen Sand samples have a higher quartz content, respectively 55 and 59%, and a lower 2:1 clay mineral content, namely 32 and 29%, in comparison to Boom Clay. The smectite content is predicted to be 13wt% for the undisturbed and 14 wt% for the disturbed sample, which are expected results for a sandy formation. The values also resemble the values of the reference sample K17 of Jacops et al. (2017), which has a quartz content of 55% and a 2:1 clay content of 27%.

Besides the two dominant components, quartz and 2:1 clay minerals, other mineral components are present in a lower concentration. Minor minerals are kaolinite, 8% in NaNi and 2 $\pm$ 0.2% in Mol2A, plagioclase, 2.5% in NaNi and 4.1% in Mol2A and orthoclase, 2.2% in NaNi and 4.9 $\pm$ 0.5% in Mol2A.

The nitratine content, a mineral occurring from the precipitation of $NaNO_3$ is also measured during the XRD-analysis to evaluate whether the percolation of the samples with $NaNO_3$ has a great impact on the mineralogical composition of the samples. The conclusion is that the mineral concentration of nitratine remains sufficiently low in the disturbed

samples and the overall mineralogical composition is not affected by the perturbation of $NaNO_3$ in the Boom Clay or in the Eigenbilzen Sand.

The specific surface area is given in Table 3. The measurements are taken with the TriStar II 3020, which analyses the quantity of adsorbed N_2. The isotherms of Boom Clay, disturbed NaNi H4 and undisturbed reference sample K4 are shown in Figure 19. The Eigenbilzen Sand isotherms, undisturbed and disturbed Mol2A, are plotted in Figure 20. The SSA is subsequently calculated using the BET-theory. The specific surface area equates to the potential area for sorption, hence, the quantification of this parameter is of interest.

Thommes et al. (2015) presented a classification scheme for isotherms, and the isotherms for Boom Clay and Eigenbilzen Sand relate best to the type IV isotherm. Type IV is common for mesoporous absorbents. However, there is also a considerable amount of N_2 adsorbed at low relative pressure (< 0.1). In this range, adsorption indicates the presence of nanopores. Comparing Figures 19 and 20, the adsorption at low relative pressure is more important for the Boom Clay, which has a higher clay content, than for Eigenbilzen Sand.

It is remarkable that adsorption has significantly decreased after perturbation of Boom Clay and Eigenbilzen Sand. The decrease of adsorption for the perturbed NaNi H4 leads to an SSA of 24.96 m^2/g, which is almost half as low as the undisturbed K4, having an SSA of 45 m^2/g. A similar reduction of SSA is noticeable for Eigenbilzen Sand, undisturbed Mol2A has an SSA of 15.08 m^2/g and disturbed Mol2A only has an SSA half as low of 6.01 m^2/g.

Table 3: Mineralogical composition, specific surface area and micropore volume of the disturbed NaNi H4, reference sample K4, disturbed and undisturbed Mol2A-189 and reference sample K17. NM = Not Measured.

	NaNi H4 disturbed	K4	Mol2A-189 undisturbed	Mol2A-189 disturbed	K17
Quartz (%)	16,4	28	55.0	58,9	54
Orthoclase (%)	2,18	5.0	5,50	4,45	8.0
Plagioclase (%)	2,51	1.0	4,06	4,15	5.0
Pyrite (%)	2,72	2.0	0,613	0,648	0.50
Anatase (%)	1,24	0.70	0,145	0,157	NM
Nitratine ($NaNO_3$) (%)	0,52	NM	0,00	0,98	NM
Kaolinite (%)	8,01	9.0	2,22	1,90	3.0
2:1 clay (%)	66,43	49	32,3	28,85	27
Prediction wt% smectitic layers	26.4	20.2	14.3	13.0	12.4
Surface area (m^2/g)	24.96	45.0	15.08	6.01	20.0

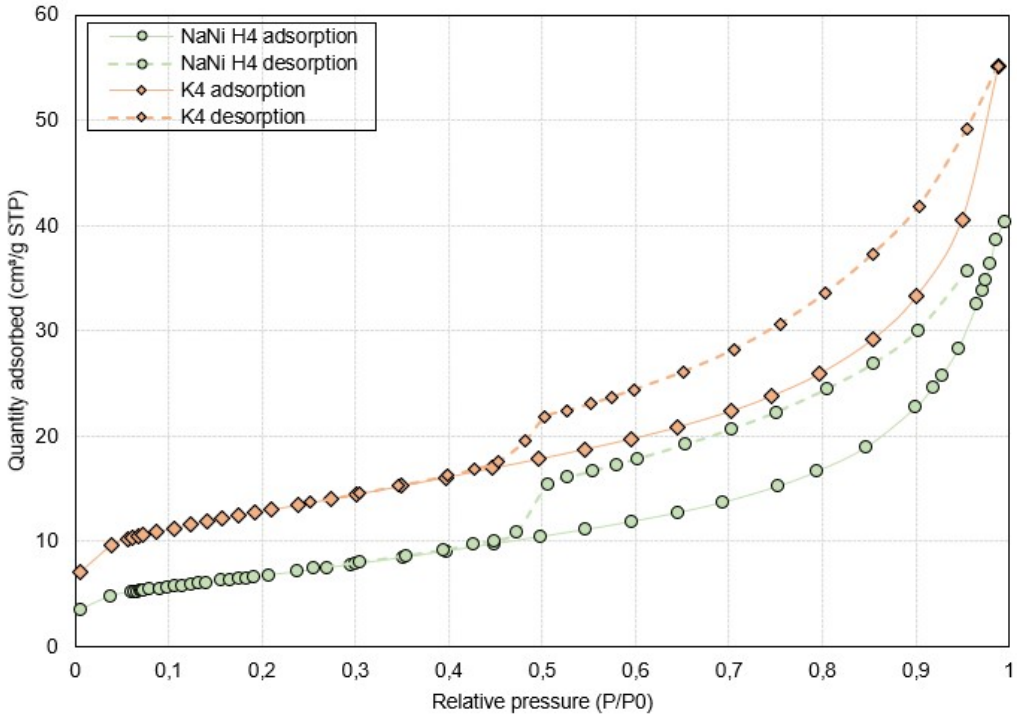

Figure 19: Isotherm of Boom Clay, the adsorbed N_2 in function of the relative pressure, in green the disturbed NaNi H4 and in orange the undisturbed K4.

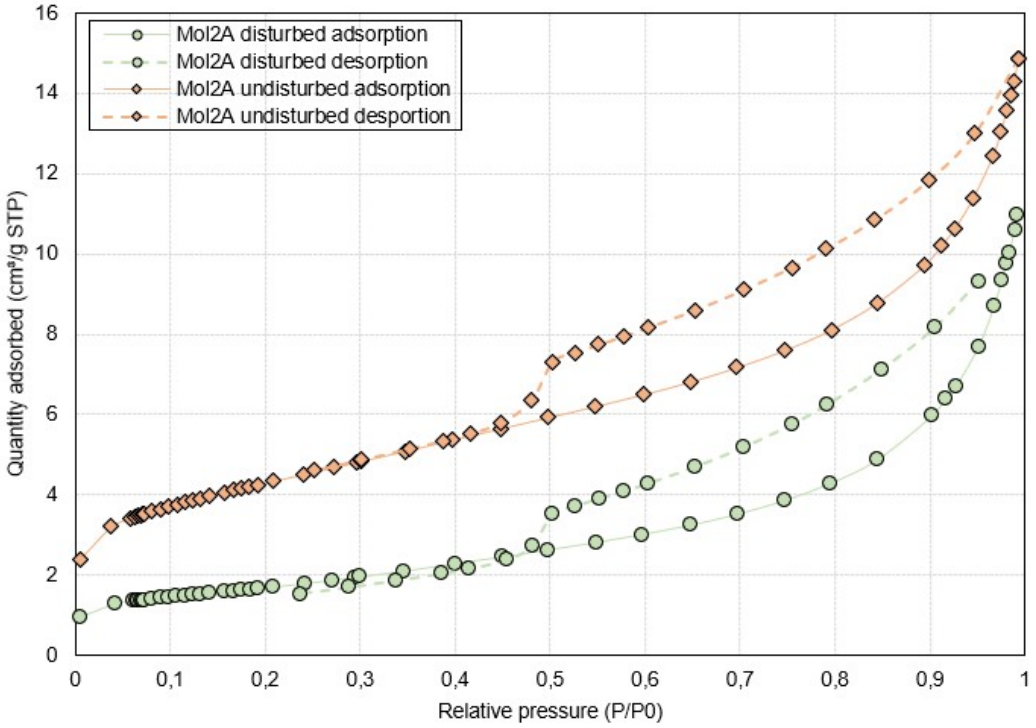

Figure 20: Isotherm of Eigenbilzen Sand, the adsorbed N_2 in function of the relative pressure, in green the disturbed Mol2A and in orange the undisturbed Mol2A.

The comparison between NaNi H4 and K4 is of course not as representative as the comparison between the perturbed Mol2A and the non-perturbed Mol2A. However, the conclusion that the SSA of Boom Clay decreases after the perturbation is also supported by comparing the data from NaNi H4 to all the data of Frederickx et al. (2018). The relation between SSA and the mineralogy is illustrated in Figure 21, where the data of (Frederickx et al., 2018) is plotted, in combination with the undisturbed reference samples K4 and K17 from Jacops et al. (2017) and Mol2A, and the disturbed NaNi H4 and Mol2A. There is a strong positive correlation between the clay content of 2:1 clay minerals and SSA.

NaNi H4 having a higher 2:1 clay concentration and a lower quartz content than Mol2A has a higher SSA. However, the measured SSA of both disturbed samples is strongly reduced in comparison to the data from the literature. NaNi H4 is expected to have a very high SSA, as this Putte-Terhaegen Member sample is very clay-enriched.

The only explanation for the drastic decrease of SSA after percolation of $NaNO_3$ is that the microstructure is influenced by this geochemical perturbation. More specifically, a blocking of the interlayers of smectite could explain the significant lowering of specific surface area. The clay stacks appear to be affected, and the N_2 is obstructed to be adsorbed on the clay surface. A hypothesis could be that there is physico- chemical obstruction in the interlayer due to the NO_3 concentration, which is the reason for the decreased D_{eff} of He. The theory that the smallest diffusing molecules, as He and HTO, take the interlayer as kind of a 'highway' could be supported by this observation (Bourg et al., 2006; Gadikota et al., 2017). Because after perturbation of $NaNO_3$, it appears that the interlayer was seriously affected by a this obstruction in the clay platelets, blocking the passage of the small diffusing molecules, as He. However, the decrease of the interlayer has no impact on the larger diffusion molecules C_2H_6 and Xe, since these molecules do not use the interlayer as a pathway but they use the mesopores to diffuse. Therefore, D_{eff} was not drastically changed for these gases.

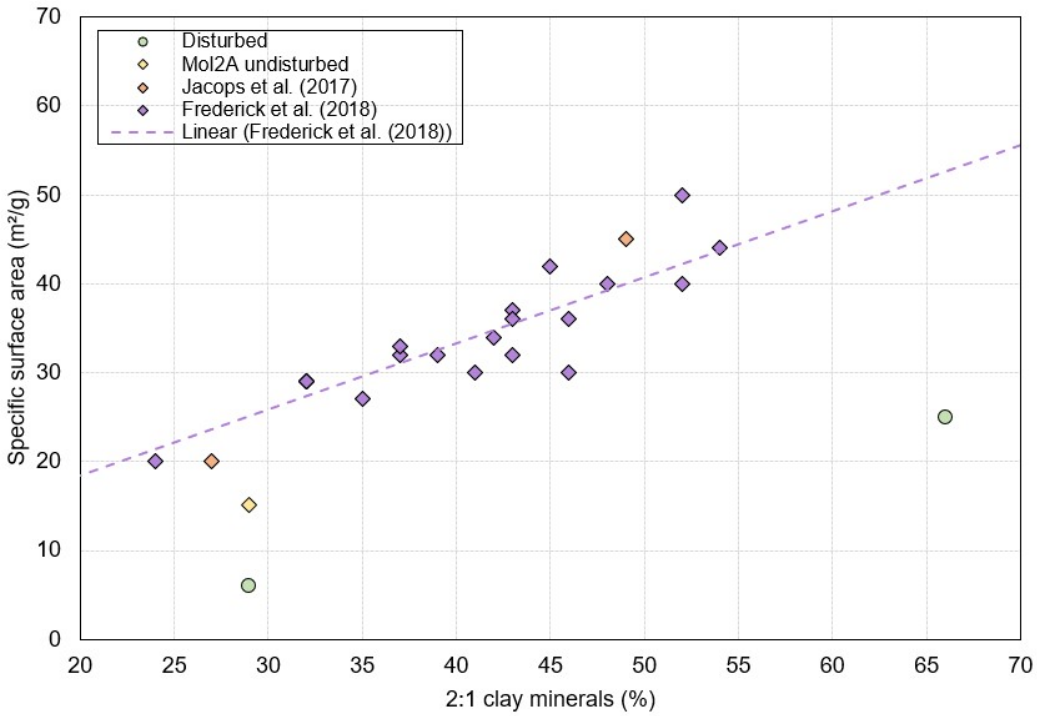

Figure 21: Relationship between the specific surface area and 2:1 clay percentage. Reference samples K4 and K17 from Jacops et al. (2017) are plotted in orange, data from Frederickx et al. (2018) in purple, disturbed NaNi H4 and Mol2A in green and undisturbed Mol2A in yellow.

6.6 Impact of $NaNO_3$ on CEC

The cation exchange capacity is an important characteristic as it gives information about the ability to adsorb cations in a form that they can rapidly be desorbed by competing ions (Bache, 1976). The CEC data is necessary since it gives the Na^+-occupancy, which is a crucial characteristic, to evaluate if the samples were percolated enough with $NaNO_3$. The aim was to have a sodium occupancy of 90%, therefore the pore volume of Mol2A had to be replaced at least 10 times (Wang, 2022). In reality, the pore volume was replaced over 15 times. The percolation of NaNi has taken place over 20 years and countless pore volumes were replaced.

In Table 4, the results from CEC measurement based on the Cu-trien difference are given. Two subsamples of NaNi (2 g and 3 g) were not considered in the final results, as the obscuration of the samples was too high. Both of the subsamples had atypical values, one turned out very brown and the other completely transparent. A transparent color normally means that the Cu-trien complex is entirely adsorbed by the clay, corresponding to extremely high CEC values. However, this result is contradicted by the realistic, ex-

pected values of CEC from the 1 g subsample. Perhaps, the NO_3 reacts with Cu-trien in a complexation reaction as soon as a certain threshold is exceeded, therefore the reaction occurs only in the 2 g and 3 g subsamples and not in the 1 g subsample.

The average CEC determined for NaNi is 27.6 ± 3.6 cmol(+)/kg and for Mol2A-disturbed 9.7 ± 0.33 cmol(+)/kg. These values are in the expected range for Boom Clay and Eigenbilzen Sand. The CEC of Putte-Member in Frederickx et al. (2018), has an average of 22.9 ± 0.6 cmol(+)/kg. From the CEC results, the smectitic content can be derived since Środoń (2009) reported that it is possible to calculate the whole rock smectitic content as 0.91 × CEC. The result is 25 ± 3.25 wt% for NaNi and 9 ± 0.3 wt% for Mol2A-disturbed.

The predicted smectite content derived from the XRD results corresponds rather well with the acquired smectitic content from the UV-VIS analysis (± 5 wt%).

With ICP-OS, the Na^+-occupancy of disturbed NaNi H4 and Mol2A can be measured. The results are given in Table 4. However, since $NaNO_3$ is present in the pore solution and precipitates as nitratine, it is important to perform a correction. The quantity of NO_3 is deduced from the total amount of Na, giving the amount of exchangeable Na (occupancy). As seen in the results, Na is nearly the only cation present on the clay minerals. The other cations Ca^{2+}, Mg^{2+}, and K^+ have either disappeared or are present in very small amounts. A side note must be made for these results; as there was rather a high urgency to acquire this data, the samples are measured without dilution causing the detection limit of certain elements to be greater than expected. For this reason, Na^+ was only measurable with a concentration 140 mg/l and K^+ only with a concentration 12 mg/l. This is rather problematic for the small, silt-enriched samples of Mol2A with 1 or 2 g sample material. For these samples, Na+-occupancy seems to be zero or even negative after NO_3-correction. In reality, Na has a concentration between 0 and 140 mg/l. Similar for K, which perhaps has a concentration between 0 and 12 mg/l. As a consequence, the sum of the exchangeable cations (Ca + K + Mg + Na) is a lot lower than the CEC of these silt-enriched samples. In the clay-enriched samples, NaNi H4 and the silt-enriched samples with a higher mass (2 and 3 g), the detection limits are easily exceeded and the sum of the exchangeable cations corresponds to the CEC.

The CEC results obtained with UV-VIS and ICP-OS are consistent with each other and fall in the normal range for Boom Clay and silt-enriched Eigenbilzen Sand. In conclusion, $NaNO_3$ does not have an influence on the cation exchange capacity and Na+ is practi-

cally the only cation remaining. Hence, the percolation of the samples with $NaNO_3$ was successful. These are the exact same conclusions as taken in Bleyen et al. (2018).

Table 4: Results of the Cu-trien experiments for disturbed NaNi H4 and Mol2A-189. All values are indicated in cmol(+)/kg and the smectitic wt% is predicted thanks to Środoń (2009)

	NaNi				Mol2A					
Quantity	3 g	1 g	2g	**average**	1g	3g	1g	2g	2g	**average**
Ca	0.0	0.9	0.0	0.3 ± 0.4	0.2	0.0	3.4	0.1	2.8	0.0 ± 0.03
K	1.1	0.0	0.0	0.4 ± 0.5	0.0	0.0	0.0	0.0	1.5	0.0 ± 0.0
Mg	0.0	0.0	0.0	0.0 ± 0.0	0.0	0.0	0.0	0.0	0.0	0.0 ± 0.0
Na	25.9	30.7	29.5	28.7 ± 2.1	-19.1	9.5	0.0	10.4	0.0	10.0 ± 0.4
Cu (=CEC)	16.6	30.1	24.9	23.8 ± 5.6	9.4	9.7	9.4	9.7	9.1	9.7 ± 0.02
SUM	26.9	31.6	29.5	29.3 ± 1.9	-18.9	9.5	3.4	10.5	2.8	10.0 ± 0.05
CEC (Cu)	16.6	30.1	24.9	23.8 ± 5.6	9.4	9.7	9.4	9.7	4.3	9.7 ± 0.02
CEC (UV VIS)	0.2	30.1	25.1	18.5 ± 13.1	9.8	10.0	10.1	9.7	9.1	9.8 ± 0.1
Smectite wt%	0.1	27.4	22.8	25 ± 3.24	8.9	9.1	9.2	8.4	8.8	9 ± 0.30

6.7 Impact of $NaNO_3$ on the pore size distribution

The results of the NMR analysis are illustrated in Figure 22. When the NMR signal is extrapolated back to zero time, in a T_2 measurement, the signal is proportional to the hydrogen concentration in the probed zone. Therefore, the NMR signal is an excellent indication of porosity as porosity is proportional to the area under the curve of the T_2-distribution. However, the intensity of the peak is also dependent on the size of the sample. So, unfortunately, the difference in intensity peak height is a side effect of the unequal size of both samples.

The T_2 curve varies with the pore structure features, and its distribution is usually highly correlated to the pore size distribution. Typically, clays have a short relaxation time, as a consequence of the high abundance of small pores, causing water to relax much faster than it would in larger pores (Testamanti & Rezaee, 2017). The T_2 component below 3 ms is associated with clay-bound water and relates to fluid in small pores. Between 3 and 33 ms, the fluid it is associated with irreducible capillary bound water and above 33 ms the fluid in larger pores is related to free fluid. This is a simplification and the boundaries are in reality not so strict and the cut-off T_2 value discriminates the free water from the capillary bound water (Dunn et al., 2002; Testamanti & Rezaee, 2017). If the grains are well sorted, the curve of T_2 displays one single peak, however when the pores are smaller than 800 nm, all the pores are gathered at one single relaxation time (Fleury & Romero-Sarmiento, 2016).

In Figure 22, the transverse relaxation time from NaNi and Mol2A is shown. The peak of NaNi at 1.86 ms indicates clay-bound water in micropores, smaller than 800 nm. Mol2A has a slightly larger relaxation time of 5.6 ms. The increase in the transverse relaxation time is a result of an increased pore size distribution in Eigenbilzen Sand.

The obtained porosity's from NaNi and Mol2A are respectively 36.57% and 22.7%. The latter is much lower than expected since Boom Clay and Eigenbilzen Sand usually have a rather similar porosity of around 38%. The obtained results is probably due to the smaller sample size of Mol2A.

The undisturbed Eigenbilzen Sand sample, Mol2A, is also measured with NMR and the peak at around 5 ms, shown in Figure 23, is very similar to the peak of the disturbed Mol2A. For the undisturbed Boom Clay samples, K4 or NaNi H4, there was, unfortunately, no NMR measurement available. For this reason, the results of NMR measurements of other Boom Clay samples are used to compare with the disturbed NaNi H4. In Figure

23, all the samples are represented and there is a clear systematic peak for every sample between 1 and 7 ms, as is the case for the disturbed Boom Clay sample.

However as explained above, pores smaller than 800 nm are accumulated in one peak. Consequently, it becomes hard to make a conclusion concerning the influence of $NaNO_3$ on the pore size distribution based on NMR data.

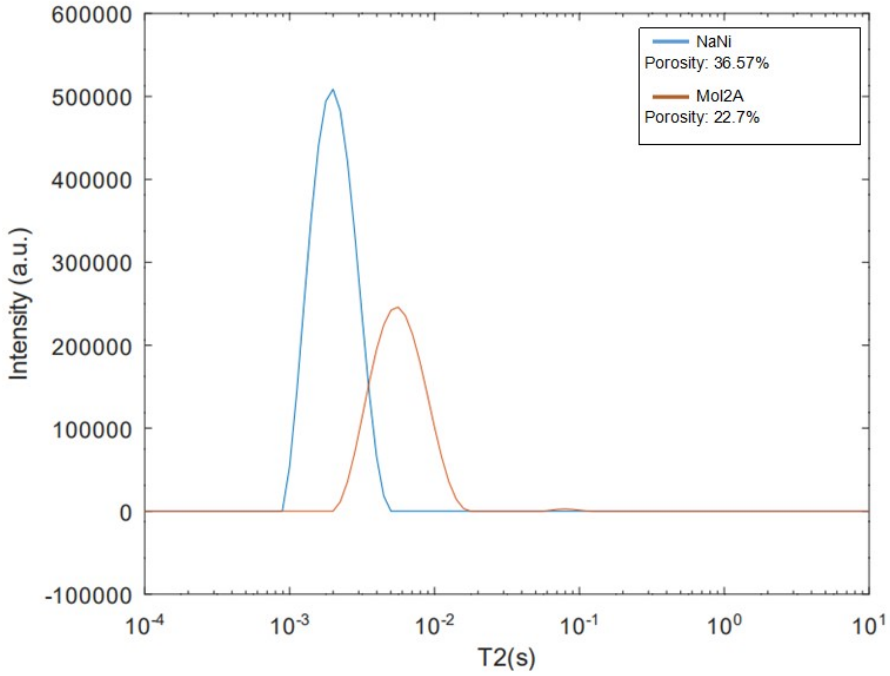

Figure 22: NMR results of NaNi and disturbed-Mol2A

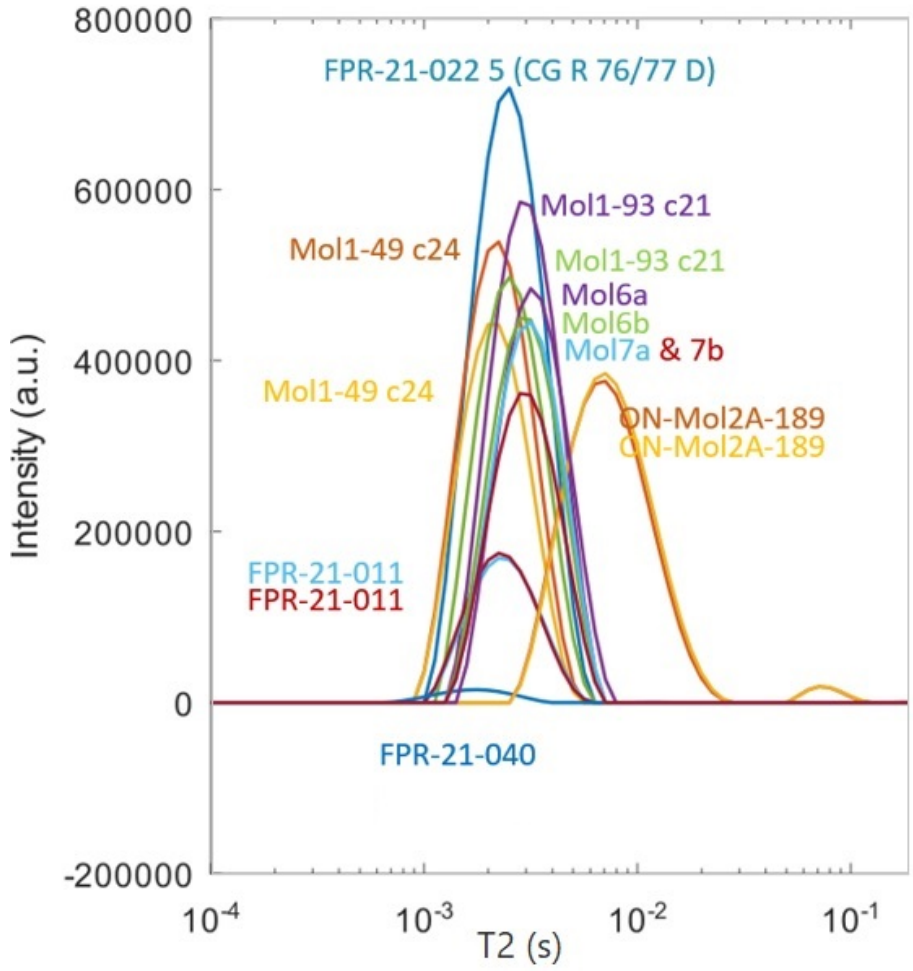

Figure 23: NMR results of different undisturbed Boom Clay and Eigenbilzen Sand results (Claes, 2022).

6.8 Missing Results and recommendations

We were planning on performing 2 more techniques to characterize the samples, unfortunately, due to some problems we did not manage to do them anymore. The first one missing is the optical microscope, the problem was to get the thin sections on time after the diffusion experiment. We wanted to include the results of microscopy to have information on the distribution of the mineral phases, however thanks to the XRD data we know the mineralogical composition and the mineral quantity. We also planned on using Mercury intrusion porosimetry (MIP), unfortunately, there were some troubles finding a free date in the months of April/May and finding someone who could assist me. With MIP, we would have gotten some information about the pore size distribution, but we don't know if these results would have been an added value since our clay samples were small and plastic, the measurements would have been influenced by that. Also, we have information on the pore size distribution thanks to N_2-adsorption and NMR.

What could be very interesting in further research is Transmission Electron Microscopy (TEM). This gives direct images with resolutions of 0.2 nm and is capable of resolving very fine structures. With TEM, the in situ distribution and character of the pore network can be determined, as the mineralogical and clay micro fabrics. It could give an image of the clay platelets and interlayers to examine if the perturbations are visible on this level.

7 Conclusion

Boom Clay is studied as a potential host rock for geological disposal of radioactive waste. It is important to understand the transport properties of gases and radionuclides in Boom Clay, as these are decisive whether or not Boom Clay is appropriate as host rock. The behaviour of gases, radionuclides, and fluids in undisturbed Boom Clay has been analysed in previous studies and had a positive outcome for geological disposal. The problem studied in this thesis research is geochemical perturbation of Boom Clay due to $NaNO_3$ caused by leaching of bituminised waste.

More specifically, the effect of $NaNO_3$ on advective and diffusive transport behaviour is evaluated. This is done by respectively measuring the hydraulic conductivity and the diffusion coefficient of 4 gases (He, CH_4, Xe, C_2H_6). For the latter, the double-through diffusion experiment is used, this is a setup based on Jacops et al. (2013). The diffusion experiment of this thesis research was successfully performed on 3 samples; disturbed Boom Clay 'NaNi H4', disturbed Eigenbilzen Sand 'Mol2A' and undisturbed Eigenbilzen Sand 'Mol2A'. With the results of the diffusion experiment, the diffusion coefficient could be calculated based on the diffusion transport model. The obtained diffusion coefficients in disturbed clay were compared to diffusion coefficients obtained in previous studies in undisturbed samples. We concluded that after geochemical perturbation, the diffusion coefficients are decreased and that diffusive transport is affected by $NaNO_3$. On the other hand, $NaNO_3$ had no impact on the hydraulic conductivity. Because of this finding, there is a definitive discrepancy between advective and diffusive transport in Boom Clay, that could be explained by a change on microstructure level. On the grounds that $NaNO_3$ especially had an impact on the diffusion coefficient of the smallest diffusing molecule, He.

After the diffusion experiment, we characterized the samples to link possible petrographical and petrophysical changes as a result of $NaNO_3$ perturbation to the transport modifications. The porosity did not change after disturbing Boom Clay or Eigenbilzen Sand. The mineralogical composition was not influenced. The perturbed Boom Clay sample, NaNi H4, was very clay-enrich with 66% 2:1 clay minerals (illite, smectite, illite-smectite mixture and muscovite), which is typical to the Putte-Terhaegen Member. The perturbed and unperturbed Eigenbilzen Sand, Mol2A, were both more quartz-enriched with an average of 57%.

The specific surface are, relevant for characterisation of the samples, as it tells us the remaining potential area for sorption after perturbation is extremely sensitive to $NaNO_3$ because this area is twice as low as the expected, undisturbed values. We suspect that this

is caused by an obstruction in the interlayer, affecting the pathway in the clay platelets.

According to Jacops (2018), reduction of the specific surface area could have a direct influence on the advective transport, but this is something we did not witness. We learned that the diffusion coefficients were more influenced by this reduction of specific surface area and in particular, the diffusion coefficient of the smallest diffusing molecule, He. Therefore, we do believe that He uses the interlayer as a pathway for diffusion-driven transport. Hence, when the interlayer is obstructed, the passage of He is blocked as a result of less space.

The CEC is an even more important characteristic, as it is a direct measurement of cation adsorption, and is not influenced by NO_3.

So to conclude, we observe some changes in diffusive transport after disturbing Boom Clay, however, these changes are of very limited scale.

References

Aertsens, M., Govaerts, J., Maes, N., & Van Laer, L. (2012). Consistency of the strontium transport parameters in boom clay obtained from different types of experiments: accounting for the filter plates. *MRS Online Proceedings Library*, *1475*(1), 583–588.

Altmann, S., Tournassat, C., Goutelard, F., Parneix, J.-C., Gimmi, T., & Maes, N. (2012). Diffusion-driven transport in clayrock formations. *Applied Geochemistry*, *27*(2), 463-478. (Fundamental processes of radionuclide migration in the geosphere)

Bache, B. W. (1976). The measurement of cation exchange capacity of soils. *Journal of the Science of Food and Agriculture*, *27*(3), 273–280.

Bel, J. J., Wickham, S. M., & Gens, R. M. (2006). Development of the supercontainer design for deep geological disposal of high-level heat emitting radioactive waste in belgium. *MRS Proceedings*, *932*, 122.1. doi: 10.1557/PROC-932-122.1

Bergaya, F., & Lagaly, G. (2013). *Handbook of clay science*. Newnes.

Berkowitz, B., Dror, I., & Yaron, B. (2008). *Contaminant geochemistry; interactions and transport in the subsurface environment* (1. Aufl. ed.). Berlin, Heidelberg: Springer.

Bini, F., Pica, A., Marinozzi, A., & Marinozzi, F. (2019). A 3d model of the effect of tortuosity and constrictivity on the diffusion in mineralized collagen fibril. *Scientific reports*, *9*(1), 1–14.

Bleyen, N., Mariën, A., & Valcke, E. (2018). *The geochemical perturbation of boom clay due to the nano3 plume released from eurobitum bituminised radioactive waste: status 2013: Topical report* (No. ER-0221). Studiecentrum voor Kernenergie. (Score=2)

Bleyen, N., Vasile, M., Mariën, A., Bruggeman, C., & Valcke, E. (2016). Assessing the oxidising effect of nano3 and nano2 from disposed eurobitum bituminised radioactive waste on the dissolved organic matter in boom clay. *Applied geochemistry*, *68*, 29–38.

Boudreau, B. P. (1996). The diffusive tortuosity of fine-grained unlithified sediments. , *60*(16), 3139–3142.

Bourg, I. C., Sposito, G., & Bourg, A. C. M. (2006). Tracer diffusion in compacted, water-saturated bentonite. *Clays and clay minerals*, *54*(3), 363–374.

Bradbury, M. H., & Baeyens, B. (2002). *Porewater chemistry in compacted re-saturated mx-80 bentonite: Physico-chemical characterisation and geochemical modelling* (Tech. Rep.). Paul Scherrer Institute PSI.

Bruggeman, C., Maes, N., Aertsens, M., & De Canniere, P. (2009). Tritiated water retention and migration behaviour in boom clay. *SFC1 level*, *5*.

Bruggeman, C., Maes, N., Aertsens, M., Govaerts, J., Martens, E., Jacops, E., ... Van Ravestyn, L. (2010). Technetium retention and migration behaviour in boom clay. *External Report. Mol, Belgium, SCK• CEN. SCK• CEN-ER-101*.

Claes, H. (2022, May). private communication.

De Cannière, P., Maes, A., Williams, S., Bruggeman, C., Beauwens, T., Maes, N., & Cowper, M. (2010). Behaviour of selenium in boom clay. *External Report, SCK• CEN-ER-120*.

Dunn, K.-J., Bergman, D. J., & LaTorraca, G. A. (2002). *Nuclear magnetic resonance: Petrophysical and logging applications*. Elsevier.

Fleury, M., & Romero-Sarmiento, M. (2016). Characterization of shales using t1–t2 nmr maps. *Journal of Petroleum Science and Engineering*, *137*, 55-62.

Frederickx, L., Honty, M., De Craen, M., & Elsen, J. (2021). Evaluating the quantification of the clay mineralogy of the rupelian boom clay in belgium by a detailed study of size fractions. *Applied Clay Science*, *201*, 105954.

Frederickx, L., Honty, M., de Craen, M., Dohrmann, R., & Elsen, J. (2018). Relating the cation exchange properties of the boom clay (belgium) to mineralogy and pore-water chemistry. *Clays and clay minerals*, *66*(5), 449–465.

Gadikota, G., Dazas, B., Rother, G., Cheshire, M. C., & Bourg, I. C. (2017). Hydrophobic solvation of gases (co2, ch4, h2, noble gases) in clay interlayer nanopores. *Journal of physical chemistry. C*, *121*(47), 26539–26550.

Garavito, A. M., de Canniere, P., & Kooi, H. (2007). In situ chemical osmosis experiment in the boom clay at the mol underground research laboratory. *Physics and chemistry of the earth. Parts A/B/C*, *32*(1-7), 421–433.

Grathwohl, P. (1998). *Diffusion in natural porous media: contaminant transport, sorption/desorption and dissolution kinetics*. Boston: Kluwer Academic Publishers.

Hirschfeld, J. O., Curtis, C. F., & Bird, R. B. (1954). Molecular theory of gases and liquids. *Nihon Butsuri Gakkaishi*, *9*(4), 268.

Honty, M., Frederickx, L., Wang, L., De Craen, M., Thomas, P., Moors, H., & Jacops, E. (2022). Boom clay pore water geochemistry at the mol site: Experimental data as determined by in situ sampling of the piezometers. *Applied Geochemistry*, *136*, 105156.

Jacops, E. (2018). *Development and application of an innovative method for studying the diffusion of dissolved gases in porous saturated media.* Leuven: KU Leuven. Faculty of Science.

Jacops, E., Aertsens, M., Maes, N., Bruggeman, C., Krooss, B., Amann-Hildenbrand, A., & Swennen, R. (2017). Interplay of molecular size and pore network geometry on the diffusion of dissolved gases and hto in boom clay. *Applied Geochemistry*, *76*, 182–195.

Jacops, E., Aertsens, M., Maes, N., Bruggeman, C., Swennen, R., Krooss, B., ... Littke, R. (2017). The dependency of diffusion coefficients and geometric factor on the size of the diffusing molecule: Observations for different clay-based materials. *Geofluids*, *2017*, 1–16.

Jacops, E., Swennen, R., Janssens, N., Seemann, T., Amann-Hildenbrand, A., Krooss, B. M., ... Bruggeman, C. (2020). Linking petrographical and petrophysical properties to transport characteristics; a case from boom clay and eigenbilzen sands. *Applied clay science*, *190*, 105568.

Jacops, E., Volckaert, G., Maes, N., Weetjens, E., & Govaerts, J. (2013). Determination of gas diffusion coefficients in saturated porous media: He and ch4 diffusion in boom clay. *Applied clay science*, *83-84*, 217–223.

Jacops, E., Wouters, K., Volckaert, G., Moors, H., Maes, N., Bruggeman, C., ... Littke, R. (2015). Measuring the effective diffusion coefficient of dissolved hydrogen in saturated boom clay. *Applied geochemistry*, *61*, 175–184.

Jin, X., Yang, W., Gao, X., Zhao, J.-Q., Li, Z., & Jiang, J. (2020). Modeling the unfrozen water content of frozen soil based on the absorption effects of clay surfaces. *Water Resources Research*, *56*(12), e2020WR027482.

Jørgensen, J. C., Jacobsen, O. S., Elberling, B., & Aamand, J. (2009). Microbial oxidation of pyrite coupled to nitrate reduction in anoxic groundwater sediment. *Environmental science technology*, *43*(13), 4851–4857.

Liang, S.-Y., Lin, W.-S., Chen, C.-P., Liu, C.-W., & Fan, C. (2021). A review of geochemical modeling for the performance assessment of radioactive waste disposal in a subsurface system. *Applied sciences*, *11*(13), 5879.

Lowell, S., Shields, J. E., Thomas, M. A., & Thommes, M. (2006). *Characterization of porous solids and powders: surface area, pore size and density* (Vol. 16). Springer Science & Business Media.

Maes, N., Wang, L., Delécaut, G., Commission, E., for Research, D.-G., & Innovation. (2004). *Migration case study : transport of radionuclides in a reducing clay sediment (trancom ii). final report.* Publications Office.

Mariën, B.-N., A., & Valcke, E. (2013). The swelling of eurobitum by water uptake and its geo-mechanical consequences. (SCK•CEN-ER-218).

Matteucci, S., Yampolskii, Y., Freeman, B. D., & Pinnau, I. (2006). Transport of gases and vapors in glassy and rubbery polymers. *Materials science of membranes for gas and vapor separation*, *1*, 1–2.

Mertens, J., Vandenberghe, N., Wouters, L., & Sintubin, M. (2003). The origin and development of joints in the boom clay formation (rupelian) in belgium. In (Vol. 216, pp. 309–321). Geological Society Publishing House.

Moors, H. (2005). Topical report on the effect of the ionic strength on the diffusion accessible porosity of boom clay. *SCK CEN, Mol, Belgium, report SCK CEN-ER-02*.

Norris, S. (2017, 03). Radioactive waste confinement: Clays in natural and engineered barriers – introduction. *Geological Society, London, Special Publications*, *443*, SP443.26.

OECD. (2003). *Safir 2: Belgian rd programme on the deep disposal of high-level and long-lived radioactive waste: An international peer review.* OECD Publishing.

ONDRAF/NIRAS Research. (2012). Development and demonstration (rdd) plan for the geological disposal of high-level and/or long-lived radioactive waste including irradiated fuel if considered as waste. *State-of-the-art report ONDRAF/NIRAS*.

Perko, J., & Weetjens, E. (2011). Thermohydraulic analysis of gas generation in a disposal facility for vitrified high-level radioactive waste in boom clay. *Nuclear technology*, *174*(3), 401–410.

Qu, W., & Li, D. (2000). A model for overlapped edl fields. , *224*(2), 397–407.

Rodwell, W., Harris, A., Horseman, S., Lalieux, P., Müller, W., Ortiz Amaya, L., & Pruess, K. (1999). Gas migration and two-phase flow through engineered and geological barriers for a deep repository for radioactive waste. *EUR(Luxembourg)*.

Shaw, R. P. (2015). Gas generation and migration in deep geological radioactive waste repositories..

Środoń, J. (2009). Quantification of illite and smectite and their layer charges in sandstones and shales from shallow burial depth. *Clay Minerals*, *44*(4), 421–434.

Testamanti, M. N., & Rezaee, R. (2017). Determination of nmr t2 cut-off for clay bound water in shales: A case study of carynginia formation, perth basin, western australia. *Journal of Petroleum Science and Engineering*, *149*, 497–503.

Thommes, M., Kaneko, K., Neimark, A. V., Olivier, J. P., Rodriguez-Reinoso, F., Rouquerol, J., & Sing, K. S. (2015). Physisorption of gases, with special reference to the evaluation of surface area and pore size distribution (iupac technical report). *Pure and applied chemistry*, *87*(9-10), 1051–1069.

Tournassat, C., Steefel, C. I., Bourg, I., & Bergaya, F. (2015). *Natural and engineered clay barriers* (Vol. 6). London: Elsevier.

Valcke, E., Marien, A., Smets, S., Li, X., Mokni, N., Olivella, S., & Sillen, X. (2010). Osmosis-induced swelling of eurobitum bituminized radioactive waste in constant total stress conditions. *Journal of nuclear materials*, *406*(3), 304–316.

Valcke, E., Rorif, F., & Smets, S. (2009). Ageing of eurobitum bituminised radioactive waste: An atr-ftir spectroscopy study. *Journal of Nuclear Materials*, *393*(1), 175-185.

Van Geet, M., Bastiaens, W., & Ortiz, L. (2008). Self-sealing capacity of argillaceous rocks: Review of laboratory results obtained from the selfrac project. *Physics and Chemistry of the Earth, Parts A/B/C*, *33*, S396-S406. (Clays in Natural Engineered Barriers for Radioactive Waste Confinement)

Vandenberghe, N., De Craen, M., & Wouters, L. (2014). *The boom clay geology: From sedimentation to present-day occurrence : a review*. Royal Belgian Institute of Natural Sciences.

Vandenberghe, N., Hager, H., Bosch, M., Verstraelen, A., Steurbaut, E., Prüfert, J., & Laga, P. (2001, 01). Stratigraphical correlation by calibrated well logs in the rupel group between north belgium, the lower-rhine area in germany and southern limburg and the achterhoek in the netherlands. *Aardkundige Mededelingen*, *11*, 69-84.

Wang, L. (2022, May). private communication.

Wemaere, I., Marivoet, J., & Labat, S. (2008). Hydraulic conductivity variability of the boom clay in north-east belgium based on four core drilled boreholes. *Physics and chemistry of the earth. Parts A/B/C*, *33*(1), S24–S36.

Xuan, Q., Han, D.-H., & Luanxiao, Z. (2019). Elastic characteristics of overpressure due to smectite-to-illite transition based on micromechanism analysis. *Geophysics*, *84*(4), WA23–WA42.

Yu, L., Rogiers, B., Gedeon, M., Marivoet, J., De Craen, M., & Mallants, D. (2013). A critical review of laboratory and in-situ hydraulic conductivity measurements for the boom clay in belgium. *Applied Clay Science*, *75*, 1–12.

8 Appendices

APPENDIX 1: disturbed NaNi H4

Meting Start	Date	# days	HE Area	HE ppm	XENON Area	XENON ppm	ETHAAN Area	ETHAAN ppm
1	21-1-2022 00:00	0	0	0	0	0		
2	27-1-2022 10:15	6,43	8511,0	33,77			6347,57143	33,75429
3	4-2-2022 00:00	14	45432,571	373,72286	42179,57143	236,98	23299,4286	133,1129
4	10-2-2022 13:37	20,57	37692,6	302,5	60698,5	333,0	25360,375	145,965
5	17-2-2022 13:29	27,56	41840,4	340,7	142835,5	759,1	79364,80	482,75
6	23-2-2022 13:24	33,56	54574,5	457,9	113398,5714	540,92	43587	267,2643
7	3-3-2022 11:41	41,49	61797,6	524,4	160480,1	808,0	61745,8571	480,5371
8	11-3-2022 00:00	49,00	69920,1	589,1	180053,1	905,88	68576,4444	521,2544
9	18-3-2022 00:00	56,00	86771,3	745,00	216750,0	1100,00	77645,625	590
10	22-3-2022 09:49	60,41	88789,0	772,79	240753,4	1264,15	86835,25	536,97
11	25-3-2022 10:10	63,42	94047,7	821,19	271739,0	1424,75	105340,5	652,2183
	28-3-2022 10:10	66,42	98252,14	859,89	260704,14	1309,30	94391	675,0471

Meting Start	Date	# days	METHAAN Area	METHAAN ppm	mol/m³ P vat Xe/C2H6	mol/m³ Input FlexPDE	mol/m³ P vat He/CH	mol/m³ Input FlexPDE	
1	44582	0			9,95	0,00	10,02	0,00	
2	44588,42708	6,427083			9,20	0,00	8,75	0,00	
3	44596	14	7939,4286	295,95143	8,696	0	8,6411	0	
4	44602,56736	20,56736	8980,86	321,39	8,56	0,00	8,52	0,00	
5	44609,56181	27,56181	9971,3	345,6	8,40	0,00	8,32	0,00	new calib
6	44615,55833	33,55833	11364,667	379,62	8,31	0,00	8,21	0,00	
7	44623,48681	41,48681	14022,57	444,54	8,23	0,00	8,12	0,00	
8	44631	49	16260,00	499,18	8,08	0,00	7,98	0,00	
9	44638	56	19301,86	512,00	7,98	0,00	7,86	0,00	
10	44642,40903	60,40903	18492,25	553,72	7,86	0,00	7,76	0,00	
11	44645,42361	63,42361	21975,50	638,80	7,70	0,00	7,67	0,00	
	44648,42361	66,42361	25604,571	727,44429					

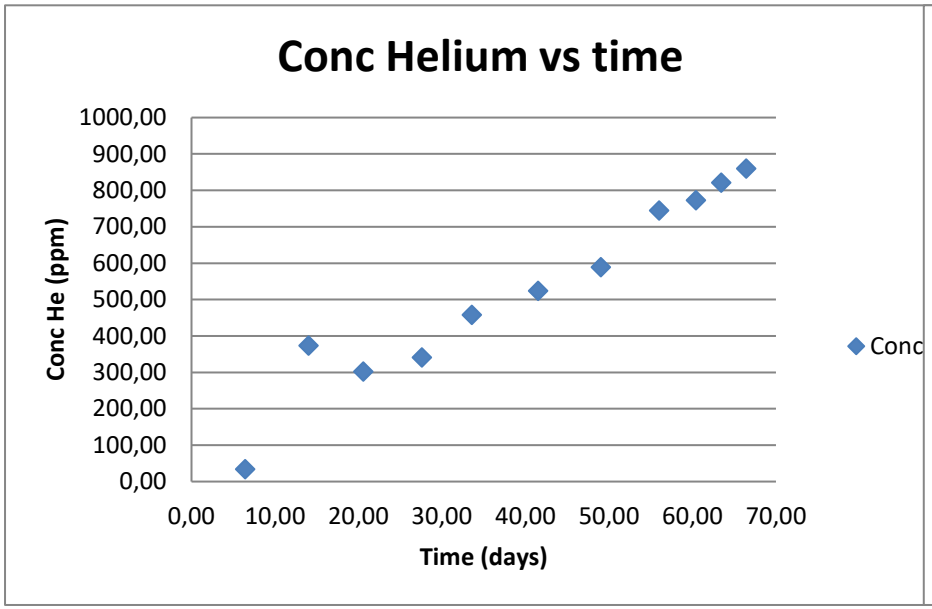
Conc Helium vs time
1000,00
900,00
800,00
700,00
600,00
500,00
400,00
300,00
200,00
100,00
0,00
Conc He (ppm)
0,00 10,00 20,00 30,00 40,00 50,00 60,00 70,00
Time (days)
Conc

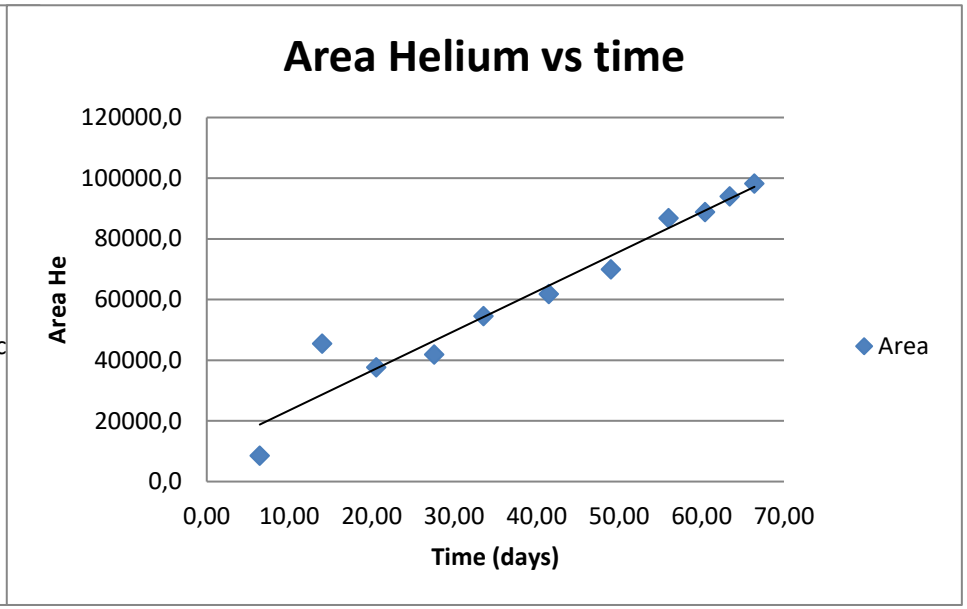
Area Helium vs time
120000,0
100000,0
80000,0
60000,0
40000,0
20000,0
0,0
Area He
0,00 10,00 20,00 30,00 40,00 50,00 60,00 70,00
Time (days)
Area

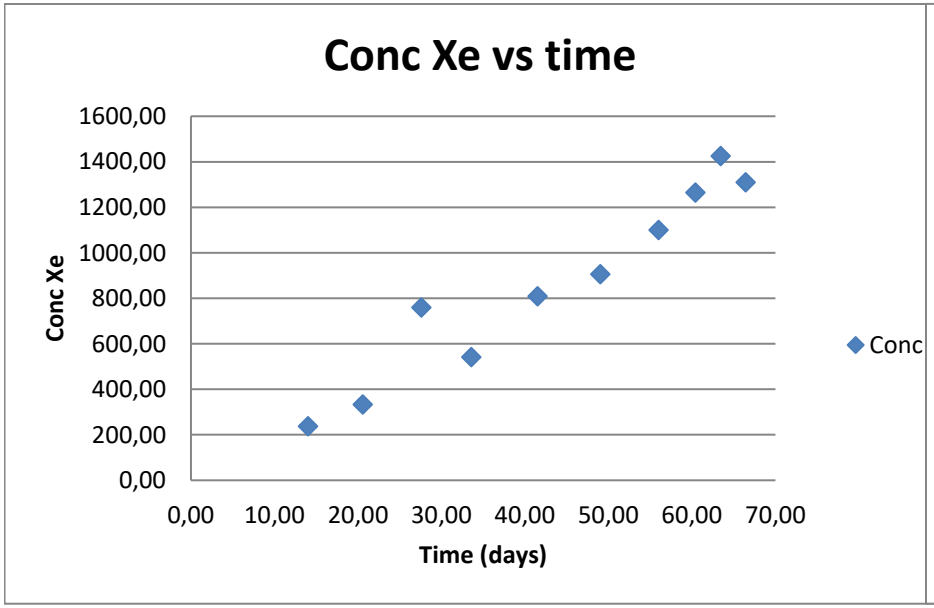
Conc Xe vs time
1600,00
1400,00
1200,00
1000,00
800,00
600,00
400,00
200,00
0,00
Conc Xe
0,00 10,00 20,00 30,00 40,00 50,00 60,00 70,00
Time (days)
Conc

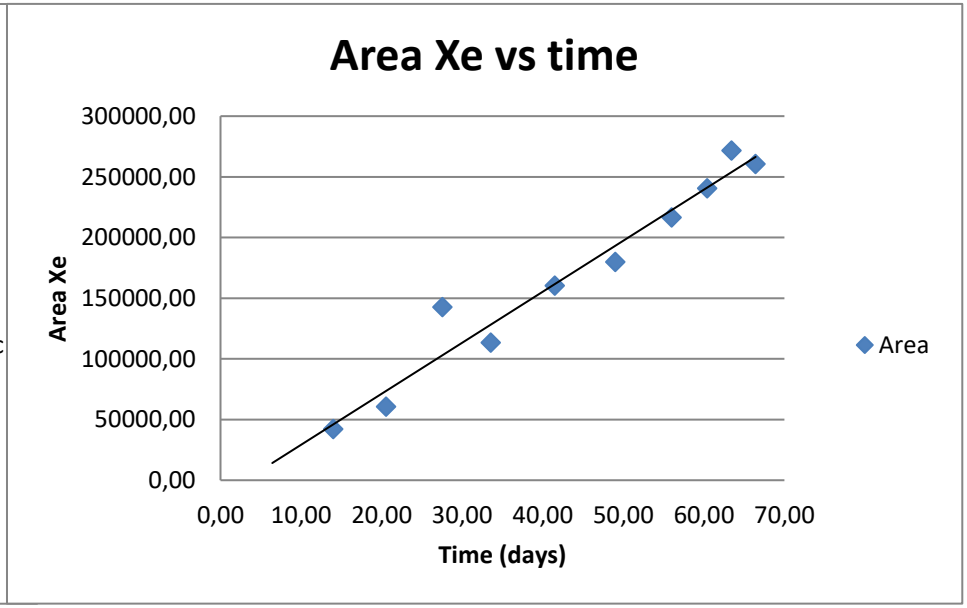
Area Xe vs time
300000,00
250000,00
200000,00
150000,00
100000,00
50000,00
0,00
Area Xe
0,00 10,00 20,00 30,00 40,00 50,00 60,00 70,00
Time (days)
Area

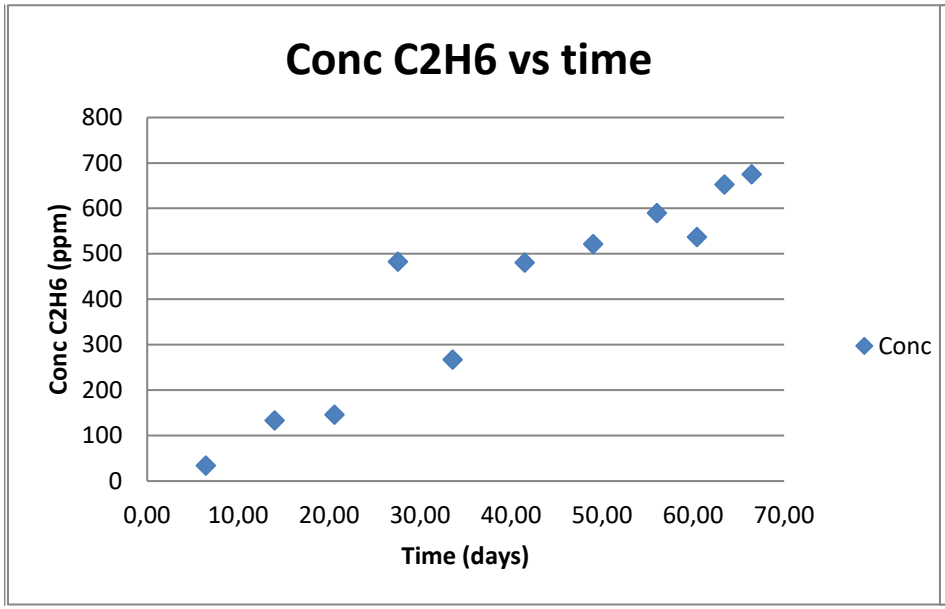
Conc C2H6 vs time
Conc C2H6 (ppm)
800
700
600
500
400
300
200
100
0
0,00
10,00
20,00
30,00
40,00
50,00
60,00
70,00
Time (days)
Conc

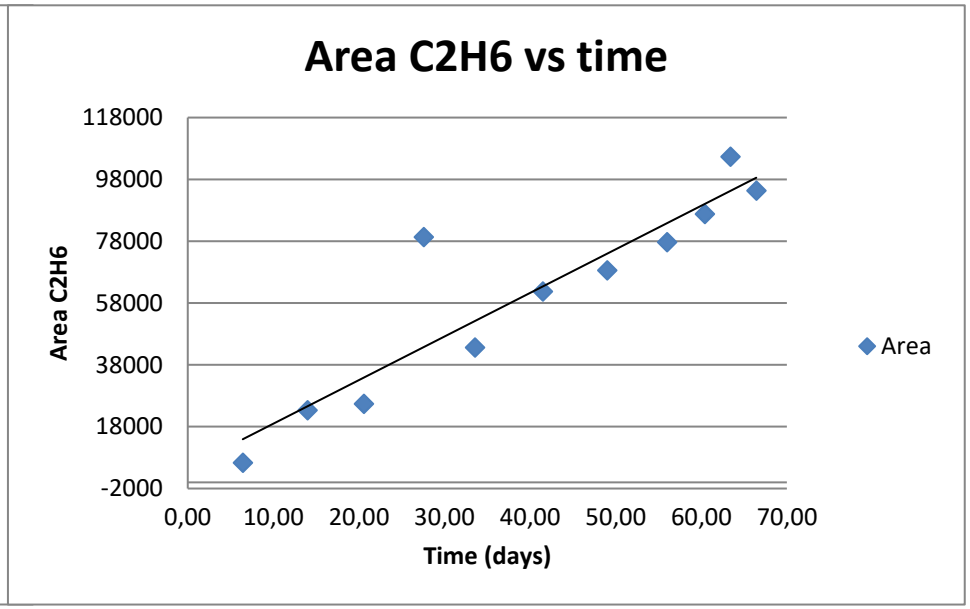
Area C2H6 vs time
Area C2H6
118000
98000
78000
58000
38000
18000
-2000
0,00
10,00
20,00
30,00
40,00
50,00
60,00
70,00
Time (days)
Area

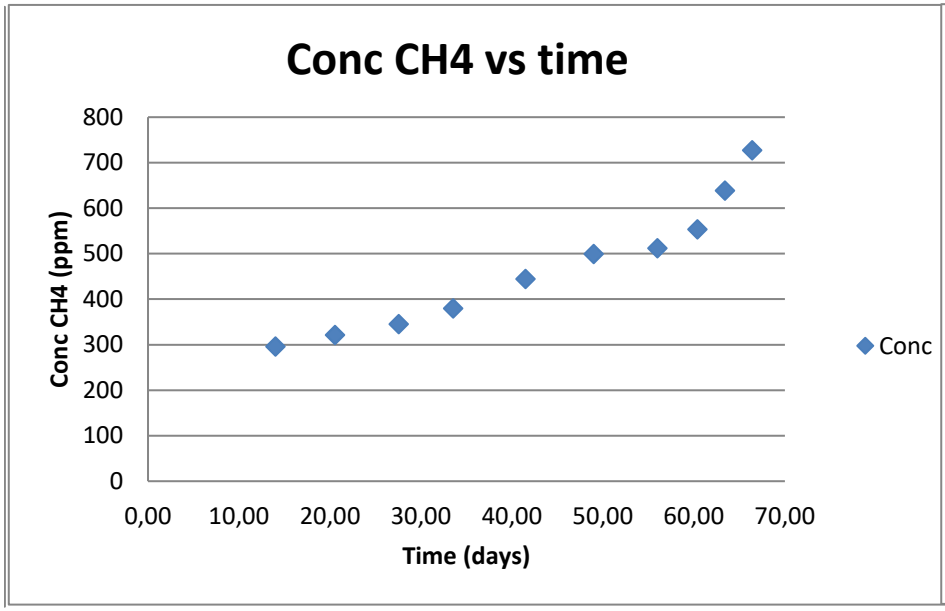
Conc CH4 vs time
Conc CH4 (ppm)
800
700
600
500
400
300
200
100
0
0,00
10,00
20,00
30,00
40,00
50,00
60,00
70,00
Time (days)
Conc

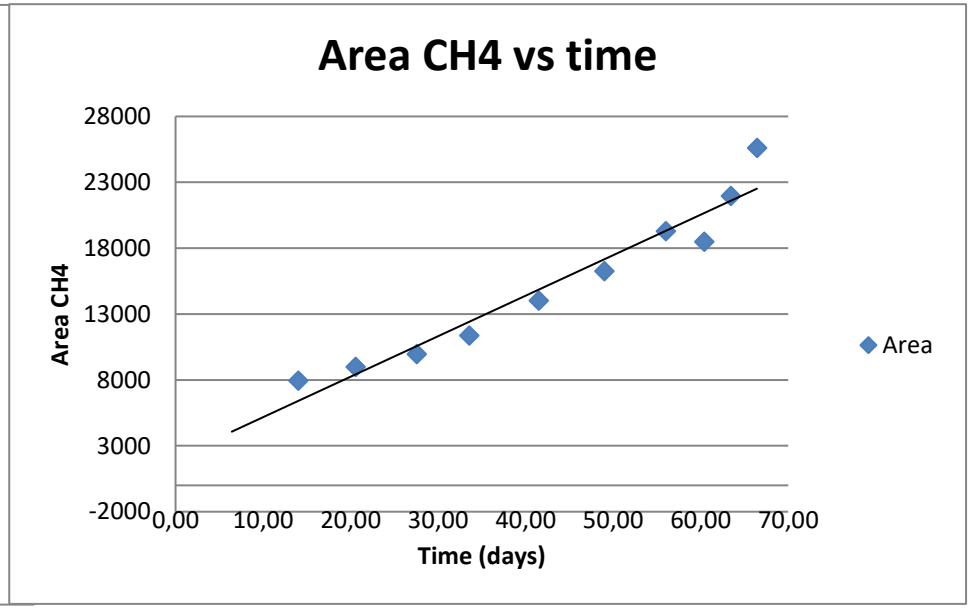
Area CH4 vs time
Area CH4
28000
23000
18000
13000
8000
3000
-2000
0,00
10,00
20,00
30,00
40,00
50,00
60,00
70,00
Time (days)
Area

APPENDIX 2: disturbed Mol2A-189

			HE		XENON		ETHAAN	
Meting	**Date**	**# days**	**Area**	**ppm**	**Area**	**ppm**	**Area**	**ppm**
Start	11-3-2022 13:40	0	0	0	0	0		
1	18-3-2022 00:00	6,43	#DIV/0!	#DIV/0!	301045,43	1511,08	109845	767,1257
2	22-3-2022 09:36	10,83055556	6917,75	19,225	360737,8	1886,016	129416	802,16
3	25-3-2022 12:45	13,96	11852,67	64,645	411325,2857	2148,207	148533,7	921,2271
4	28-3-2022 00:00	16,43	16312,14	105,69286	414285,4286	2077,506	149045	1000,69
5	30-3-2022 09:33	18,83	20874,8	147,7	463634,6667	2324,347	170043	1125,802
6	4-4-2022 09:19	23,82	27324,2	207,1	505124,8	2531,9	191954,2	1256,355
7	7-4-2022 00:00	26,43	33680,6	265,6	544569,6	2729,18	197160,3	1287,373
8	11-4-2022 00:00	30,43	41345,7	336,11	588435,4	2948,59	212666	1379,76
9	0-1-1900 00:00	-44631,57	#DIV/0!	#DIV/0!	#DIV/0!	#DIV/0!	#DIV/0!	#DIV/0!
10	0-1-1900 00:00	-44631,57	#DIV/0!	#DIV/0!	#DIV/0!	#DIV/0!	#DIV/0!	#DIV/0!

			METHAAN			mol/m³		mol/m³
			Area	**ppm**	**P vat Xe/C2H6**	**Input FlexPDE**	**P vat He/C**	**Input FlexPDE**
Meting	Date	# days			0,00	0,00	0,00	0,00
Start	44631,56944	0	0,00	0,00	0,00	0,00	0,00	0,00
1	44638	6,430555556	0,00	0,00	6,74	0	6,74	0
2	44642,4	10,83055556	2606,20	165,68	6,63	0,00	6,64	0,00
3	44645,53125	13,96180556	6112,57	247,83	6,59	0,00	6,59	0,00
4	44648	16,43055556	6633,17	264,05	0,00	0,00	0,00	0,00
5	44650,39792	18,82847222	9330,40	329,93	6,46	0,00	6,45	0,00
6	44655,38819	23,81875	10814,00	366,17	0,00	0,00	0,00	0,00
7	44658	26,43055556	13963,00	443,08	0,00	0,00	0,00	0,00
8	44662	30,43055556	#DIV/0!	#DIV/0!	0,00	0,00	0,00	0,00
9	0	-44631,56944	#DIV/0!	#DIV/0!	0,00	0,00	0,00	0,00
10	0	-44631,56944						

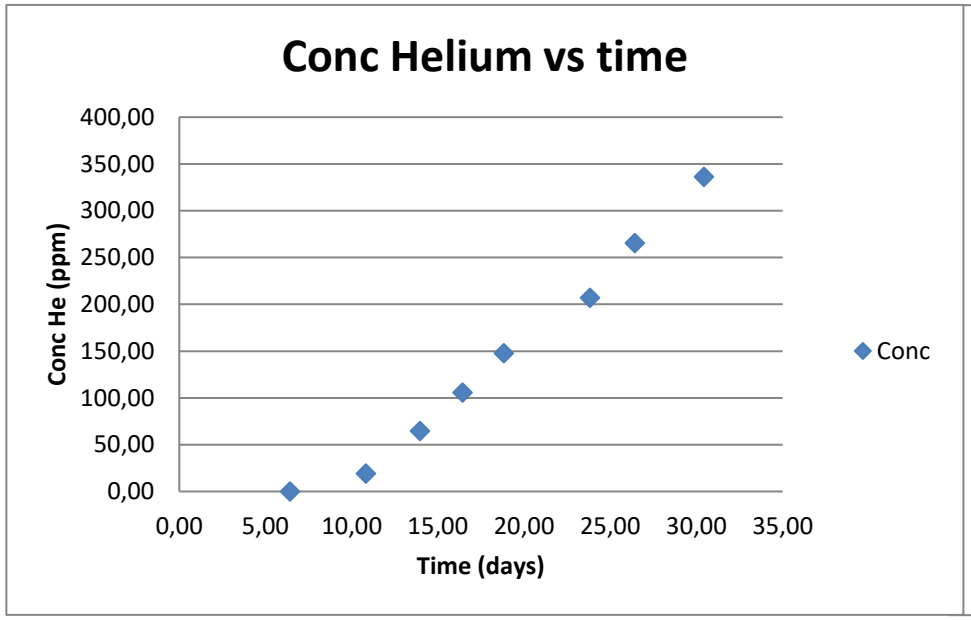
Conc Helium vs time
Conc He (ppm)
400,00
350,00
300,00
250,00
200,00
150,00
100,00
50,00
0,00
0,00 5,00 10,00 15,00 20,00 25,00 30,00 35,00
Time (days)
Conc

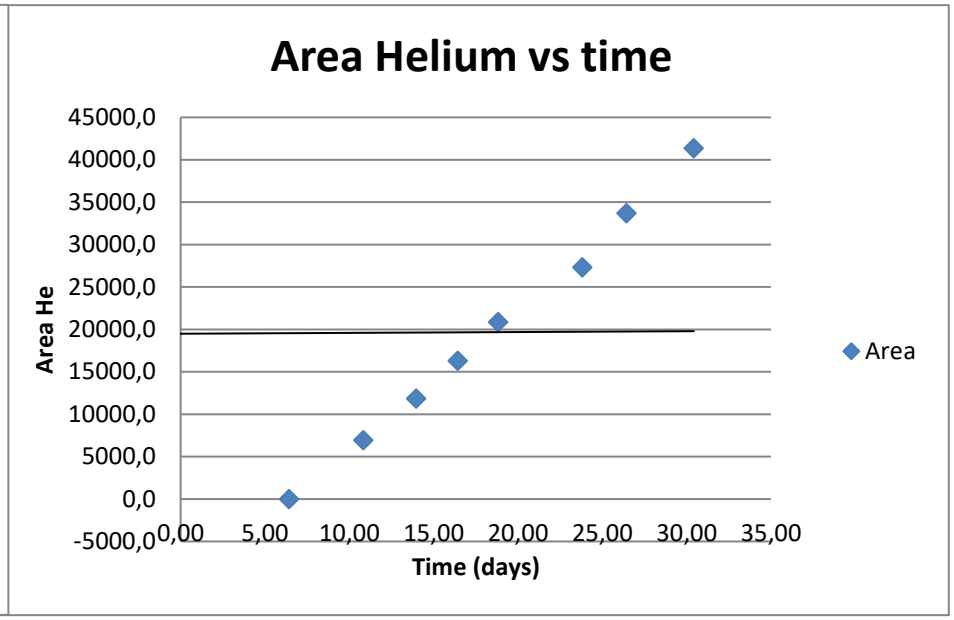
Area Helium vs time
Area He
45000,0
40000,0
35000,0
30000,0
25000,0
20000,0
15000,0
10000,0
5000,0
0,0
-5000,0
0,00 5,00 10,00 15,00 20,00 25,00 30,00 35,00
Time (days)
Area

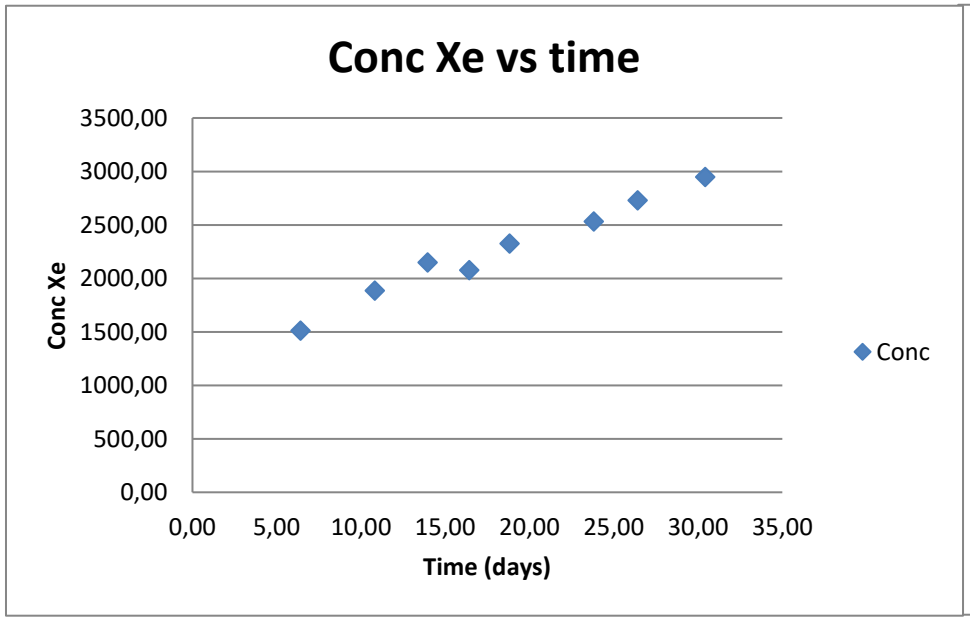
Conc Xe vs time
Conc Xe
3500,00
3000,00
2500,00
2000,00
1500,00
1000,00
500,00
0,00
0,00 5,00 10,00 15,00 20,00 25,00 30,00 35,00
Time (days)
Conc

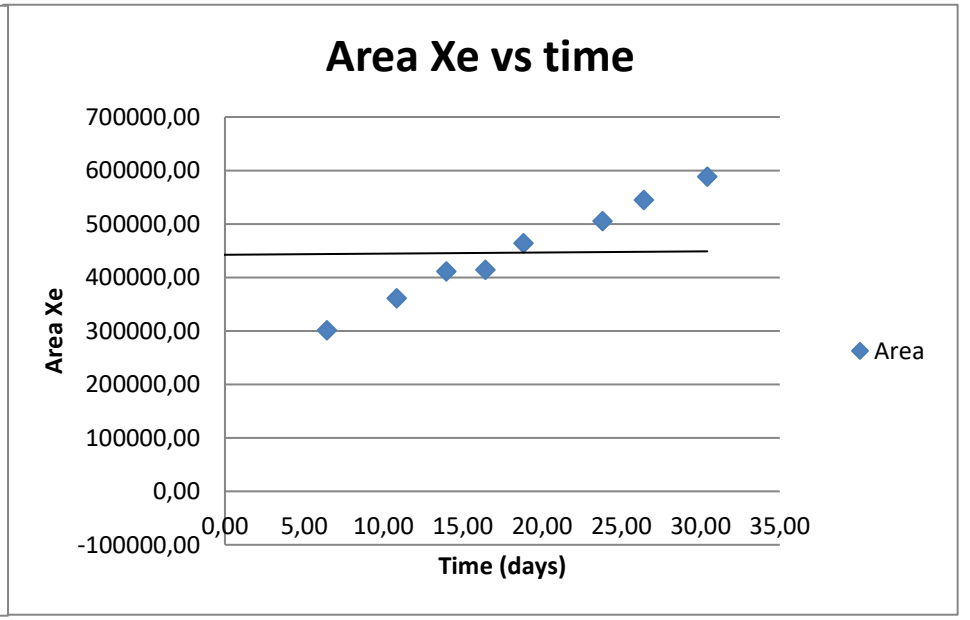
Area Xe vs time
Area Xe
700000,00
600000,00
500000,00
400000,00
300000,00
200000,00
100000,00
0,00
-100000,00
0,00 5,00 10,00 15,00 20,00 25,00 30,00 35,00
Time (days)
Area

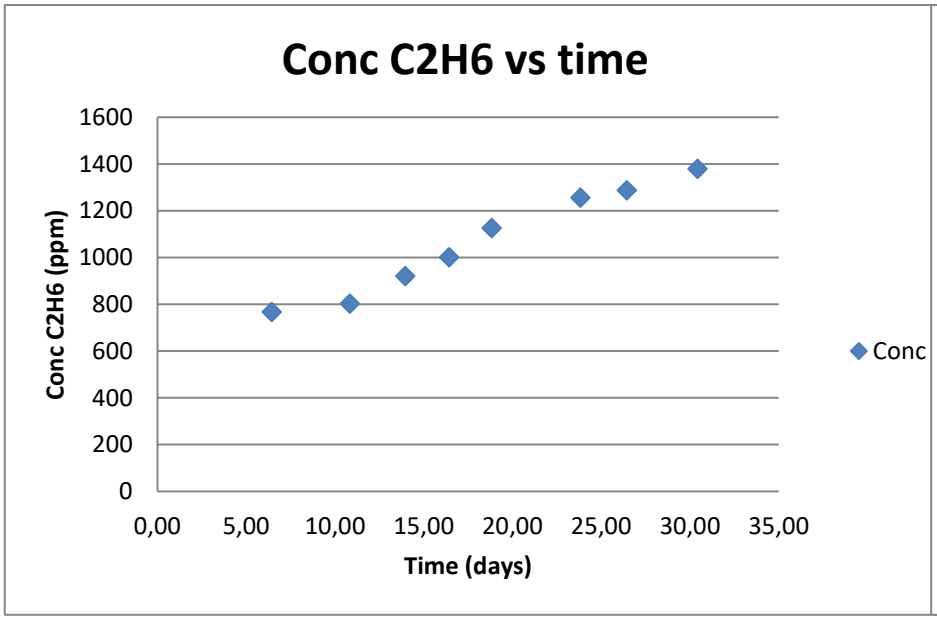
Conc C2H6 vs time
Conc C2H6 (ppm)
1600
1400
1200
1000
800
600
400
200
0
0,00
5,00
10,00
15,00
20,00
25,00
30,00
35,00
Time (days)
Conc

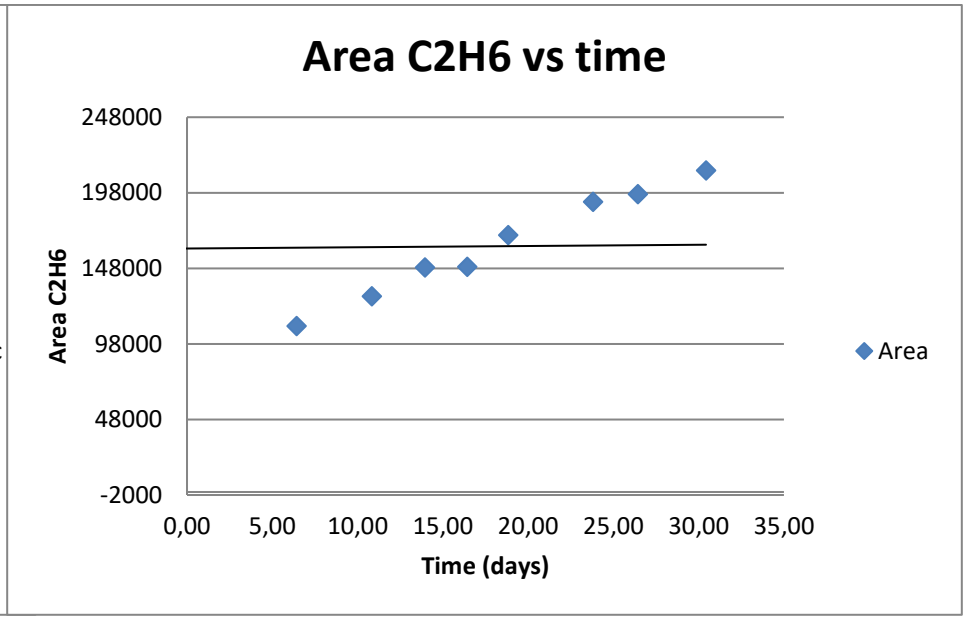
Area C2H6 vs time
Area C2H6
248000
198000
148000
98000
48000
-2000
0,00
5,00
10,00
15,00
20,00
25,00
30,00
35,00
Time (days)
Area

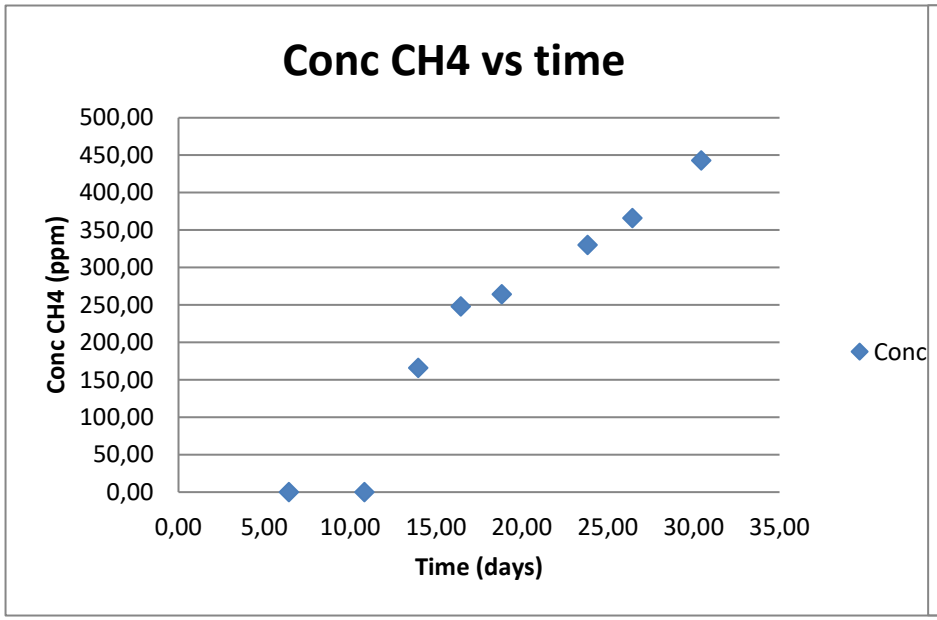
Conc CH4 vs time
Conc CH4 (ppm)
500,00
450,00
400,00
350,00
300,00
250,00
200,00
150,00
100,00
50,00
0,00
0,00
5,00
10,00
15,00
20,00
25,00
30,00
35,00
Time (days)
Conc

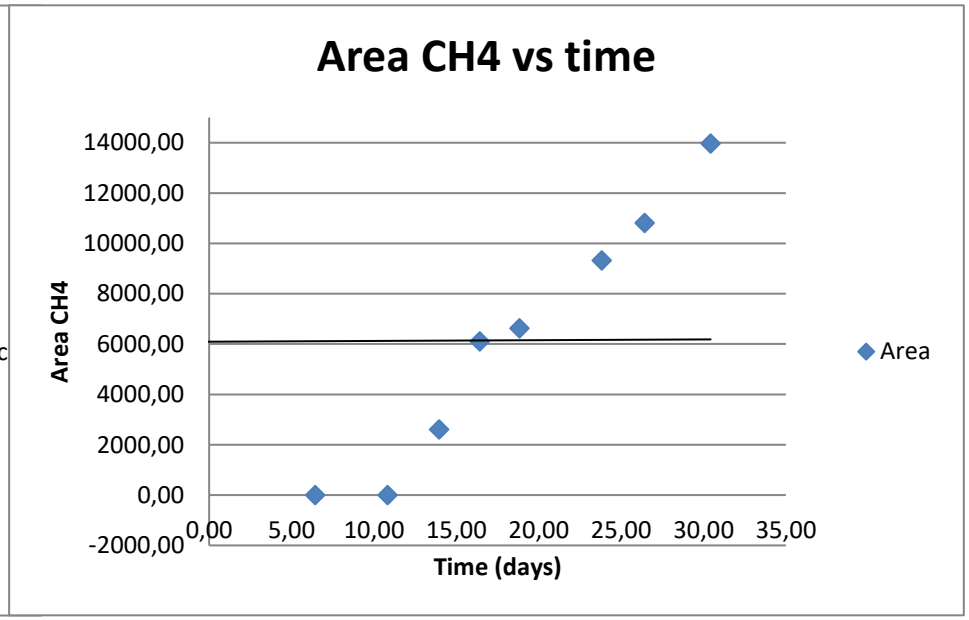
Area CH4 vs time
Area CH4
14000,00
12000,00
10000,00
8000,00
6000,00
4000,00
2000,00
0,00
-2000,00
0,00
5,00
10,00
15,00
20,00
25,00
30,00
35,00
Time (days)
Area

APPENDIX 3: undisturbed Mol2A-189

			HE		XENON		ETHAAN		
Meting	**Date**	**# days**	**Area**	**ppm**	**Area**	**ppm**	**Area**	**ppm**	**-nulstaal**
Start	19-4-2022 11:28	0	0	0	0	0			
1	22-4-2022 09:26	2,92	29025,4	222,71	6192,71	36,24	10992,86	178,1386	23,1385714
2	25-4-2022 10:55	5,977083333	33698,71	265,72286	30407,33333	157,3622	20578,33	235,25	80,25
3	29-4-2022 14:39	10,13	44995,6	369,7	79024,28571	400,5429	38194,29	340,2129	185,212857
4	2-5-2022 13:43	13,09	45407,57	373,49143	116404	587,5133	53223,88	429,76	274,76
5	6-5-2022 10:56	16,98	54613,0	458,2	149717,125	754,145	62306,25	483,8775	328,8775
6	9-5-2022 10:21	19,95	58705,1	495,9	191790,5	964,6	82769,13	605,7988	450,79875
7	12-5-2022 09:21	22,91	69177,8	592,3	220792,1	1109,66	91645,25	658,6863	503,68625
8	0-1-1900 00:00	-44670,48	#DIV/0!	#DIV/0!	#DIV/0!	#DIV/0!	#DIV/0!	#DIV/0!	#DIV/0!
9	0-1-1900 00:00	-44670,48	#DIV/0!	#DIV/0!	#DIV/0!	#DIV/0!	#DIV/0!	#DIV/0!	#DIV/0!
10	0-1-1900 00:00	-44670,48	#DIV/0!	#DIV/0!	#DIV/0!	#DIV/0!	#DIV/0!	#DIV/0!	#DIV/0!

			METHAAN			mol/m³		mol/m³
Meting	Date	# days	**Area**	**ppm**	**P vat Xe/C2H6**	**Input FlexPDE**	**P vat He/C**	**Input FlexPDE**
Start	44670,47778	0			5,95	0,00	5,95	0,00
1	44673,39306	2,915277778	5139,00	227,55	5,88	0,00	5,89	0,00
2	44676,45486	5,977083333	6006,38	248,73	5,8211	0	5,809	0
3	44680,61042	10,13263889	8491,75	309,45	5,83	0,00	8,75	0,00
4	44683,57153	13,09375	10279,13	353,10	5,70	0,00	5,69	0,00
5	44687,45556	16,97777778	13671,57	435,97	5,62	0,00	5,60	0,00
6	44690,43125	19,95347222	16400,00	502,61	5,61	0,00	5,53	0,00
7	44693,38958	22,91180556	19699,13	583,19	5,50	0,00	5,48	0,00
8	0	-44670,47778	#DIV/0!	#DIV/0!	0,00	0,00	0,00	0,00
9	0	-44670,47778	#DIV/0!	#DIV/0!	0,00	0,00	0,00	0,00
10	0	-44670,47778	#DIV/0!	#DIV/0!	0,00	0,00	0,00	0,00

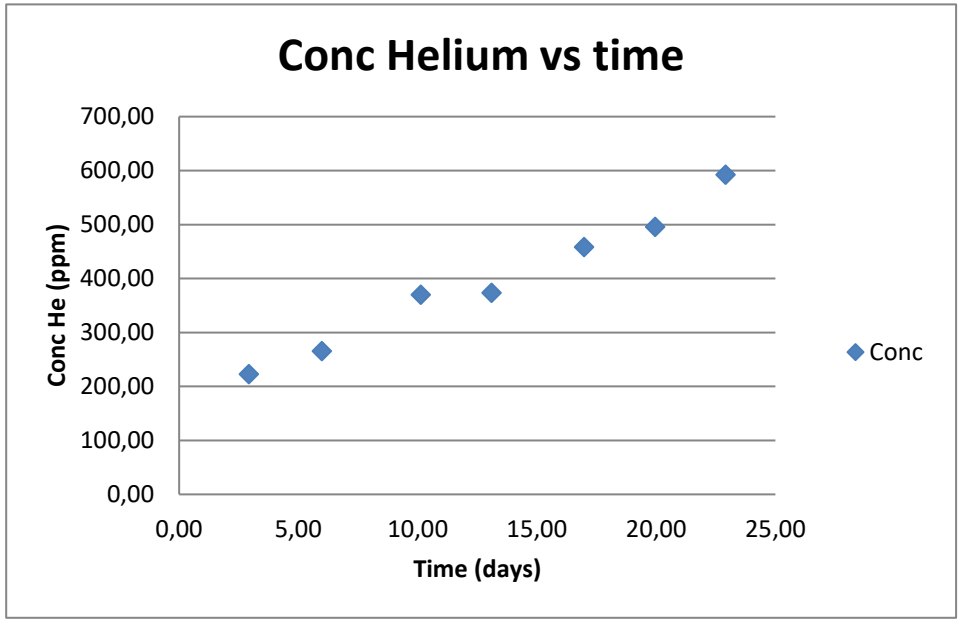
Conc Helium vs time
700,00
600,00
500,00
400,00
300,00
200,00
100,00
0,00
Conc He (ppm)
0,00
5,00
10,00
15,00
20,00
25,00
Time (days)
Conc

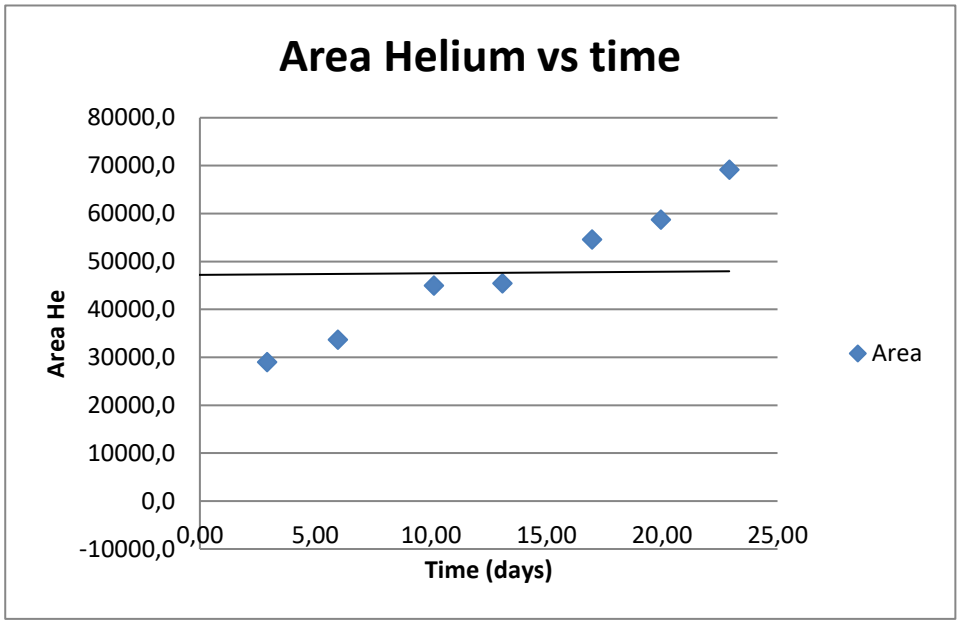
Area Helium vs time
80000,0
70000,0
60000,0
50000,0
40000,0
30000,0
20000,0
10000,0
0,0
-10000,0
Area He
0,00
5,00
10,00
15,00
20,00
25,00
Time (days)
Area

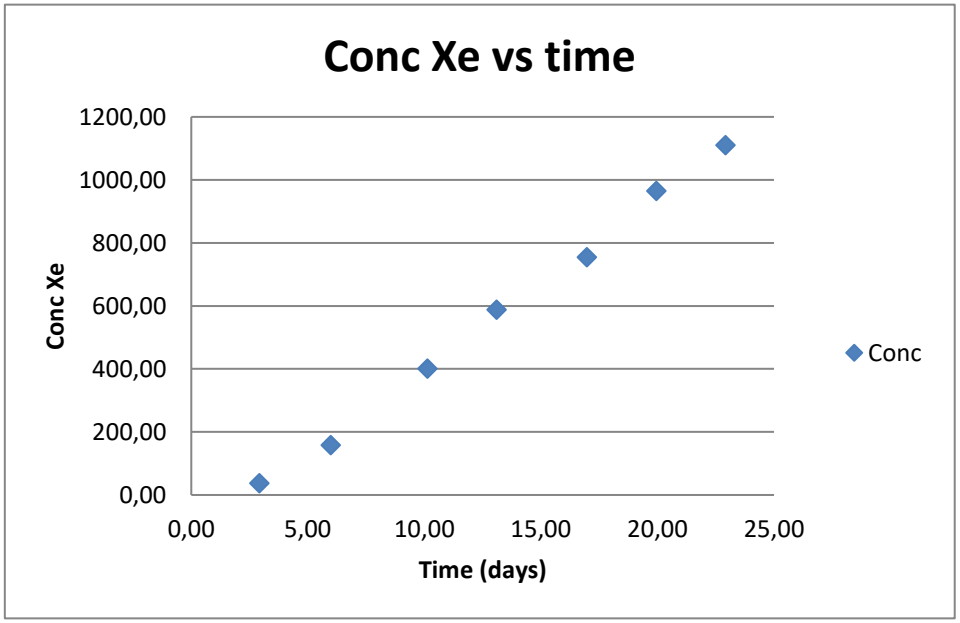
Conc Xe vs time
1200,00
1000,00
800,00
600,00
400,00
200,00
0,00
Conc Xe
0,00
5,00
10,00
15,00
20,00
25,00
Time (days)
Conc

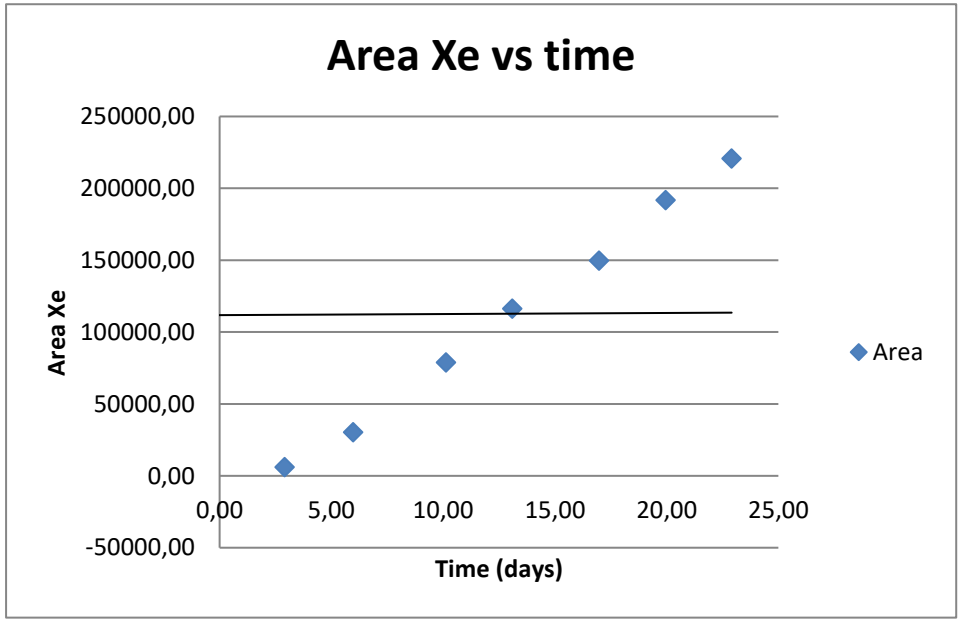
Area Xe vs time
250000,00
200000,00
150000,00
100000,00
50000,00
0,00
-50000,00
Area Xe
0,00
5,00
10,00
15,00
20,00
25,00
Time (days)
Area

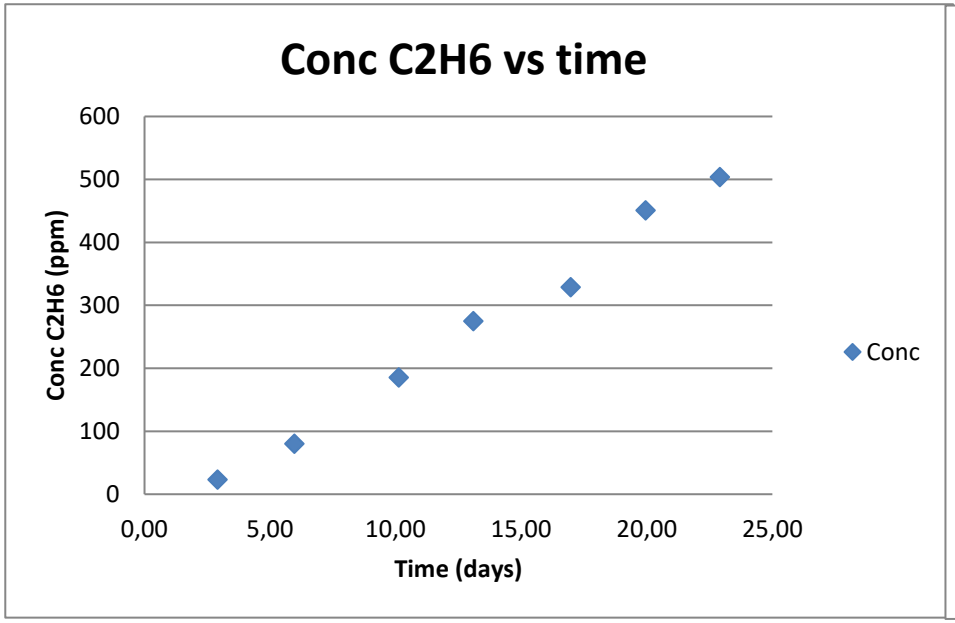
Conc C2H6 vs time
Conc C2H6 (ppm)
600
500
400
300
200
100
0
0,00
5,00
10,00
15,00
20,00
25,00
Time (days)
Conc

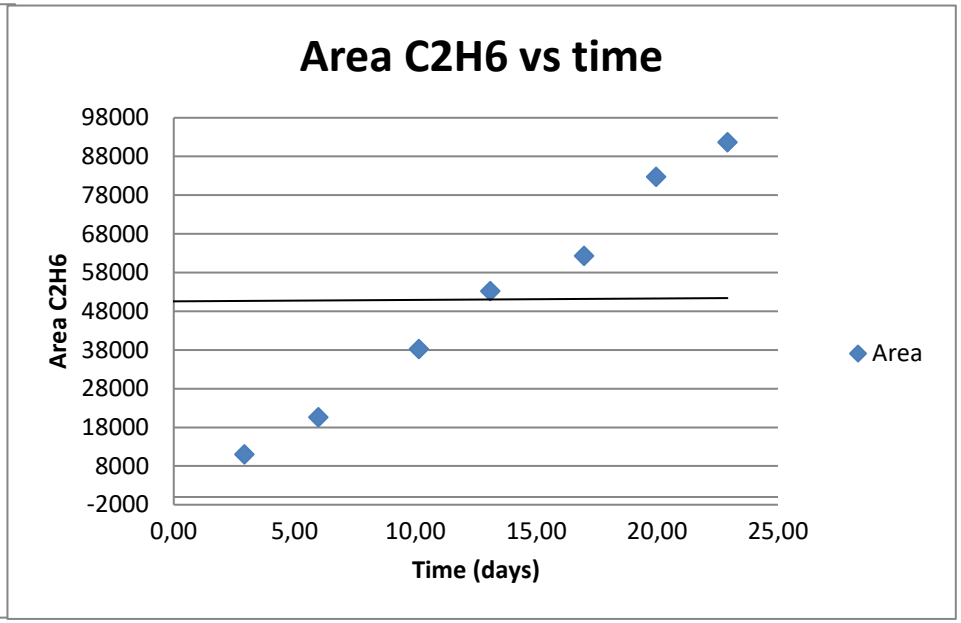
Area C2H6 vs time
Area C2H6
98000
88000
78000
68000
58000
48000
38000
28000
18000
8000
-2000
0,00
5,00
10,00
15,00
20,00
25,00
Time (days)
Area

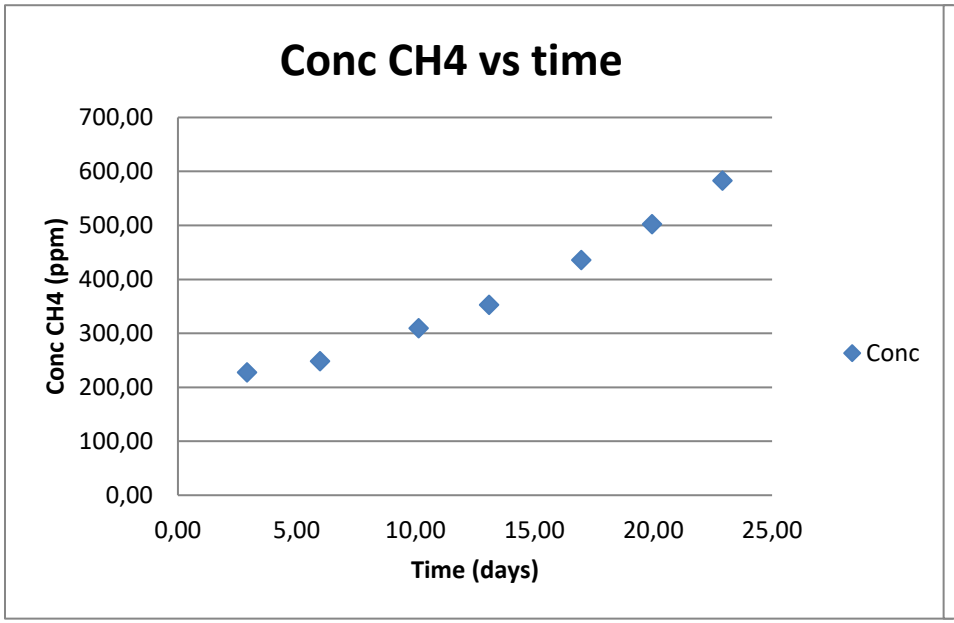
Conc CH4 vs time
Conc CH4 (ppm)
700,00
600,00
500,00
400,00
300,00
200,00
100,00
0,00
0,00
5,00
10,00
15,00
20,00
25,00
Time (days)
Conc

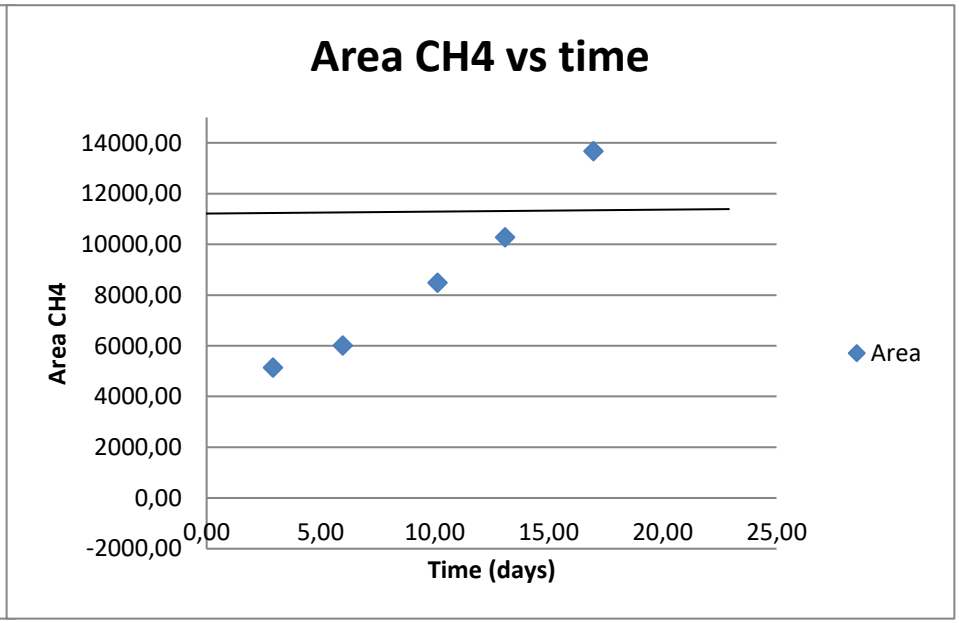
Area CH4 vs time
Area CH4
14000,00
12000,00
10000,00
8000,00
6000,00
4000,00
2000,00
0,00
-2000,00
0,00
5,00
10,00
15,00
20,00
25,00
Time (days)
Area